CHAPTER V.C

Calibration of the simultaneous growth and storage approach under aerobic conditions

Part of this chapter is published as:
Sin G., Guisasola A., Baeza J., Carrera J. and Vanrolleghem P.A. (2005). A new approach for modelling simultaneous grwoth and storage processes for activated sludge systems under aerobic conditions. Biotechnol. Bioeng. (accepted)

ABSTRACT

The model for biological COD removal presented in chapter VI.B is calibrated and validated in this chapter. To facilitate full-scale application of the model, a simple calibration methodology only based on batch OUR data is used. The model is calibrated using biomass withdrawn from two different WWTPs. These plants had biomass with very different storage capacity. The confidence intervals obtained using only OUR were too large and, after a practical identifiability analysis on the model parameters, OED was performed to gain better insight into the model structure. The OED experiment provided enough information to reduce the confidence interval values to an acceptable range.

V.C.1 Introduction

A new model to describe the simultaneous growth and storage approach for biological COD removal under aerobic condtions was developed in the previous chapter (Table V.B3). This model included titrimetric measurements to facilitate its calibration. The aim of this chapter is to calibrate this model with experimental results and to examine if this model can be fitted to different respirometric batch experiments. Several experiments are developed in this chapter with biomasses from different WWTP (operated uder different conditions) to calibrate the model. These experiments will help to discuss the most controversial issues of the storage bioprocess.

V.C.2 Experimental set-ups

The experiments of this chapter were conducted in two different experimental set-ups. On the one hand, some experiments were performed using the hybrid-respirometric set-up described in the equipments section (Chapter III.1.5) with biomass withdrawn from the Ossemerssen WWTP (Gent, Belgium). On the other hand, most of the experiments were performed in a 10 L reactor operated as an LFS type respirometer also described in the equipments section (III.A.4) with biomass withdrawn from several WWTPs from Catalonia, Spain.

The experimental methodology in both set-ups started with an overnight aeration for the biomass to reach the endogenous state. Then, a first pulse of acetate was added to induce a “wake-up” effect on the biomass activity (Vanrolleghem *et al.,* 1998). At the same time, ammonia in excess and ATU (30 mg/L) were added to avoid growth-limitation and nitrification, respectively. Once the wake-up pulse was consumed and pH was controlled, a known pulse of acetate was added to the system whereas was measured. Triplicate PHB measurements were done according to the methodology described in Pijuan *et al.*, (2004a).

Modelling, simulation and parameter estimation were performed using MATLAB 6.5 (The MathWorks, Natick, MA). The differential equations were solved using an explicit Runge-Kutta (4,5) formula. Parameter estimation was carried out by using the Nelder-Mead Simplex minimization algorithm. The confidence intervals of parameter estimates were determined using the inverse of the Fisher Information Matrix (FIM) following the methodology described in Chapter IV and in where $Y_\theta(t)$ is the so called output sensitivity function and Q_k is the inverse of the covariance matrix of the measurement noise Dochain and Vanrolleghem, (2001) [eqs. V.C1 and V.C2].

$$FIM = \sum_{k=1}^{N} Y_\theta^T(t_k) Q_k Y_\theta(t_k) \qquad \text{(V.C1)}$$

$$COV(\theta_0) \geq FIM^{-1} \qquad \text{(V.C2)}$$

V.C.3 Experimental results

V.C.3.1 EXPERIMENTAL BATCH RESPIROMETRIC PROFILES

Experiment V.C1 (Table V.C1) was conducted using biomass withdrawn from the Ossemeersen WWTP in Belgium. Figure V.C1 depicts the experimental respirometric measurements obtained after pulse addition of a certain amount of acetate to endogenously respiring activated sludge.

Table V.C1 Experiment V.C1

EXPERIMENT V.C1	Respirometric batch experiment with biomass from Ossemeersen WWTP
Equipment	Hybrid respirometer (V_0 = 3.2 L)
pH	7.8
Temperature	20 ºC
Pulses	200 mg COD as acetate (t = 5 min) -> 62.5 mg COD_{AC}/L

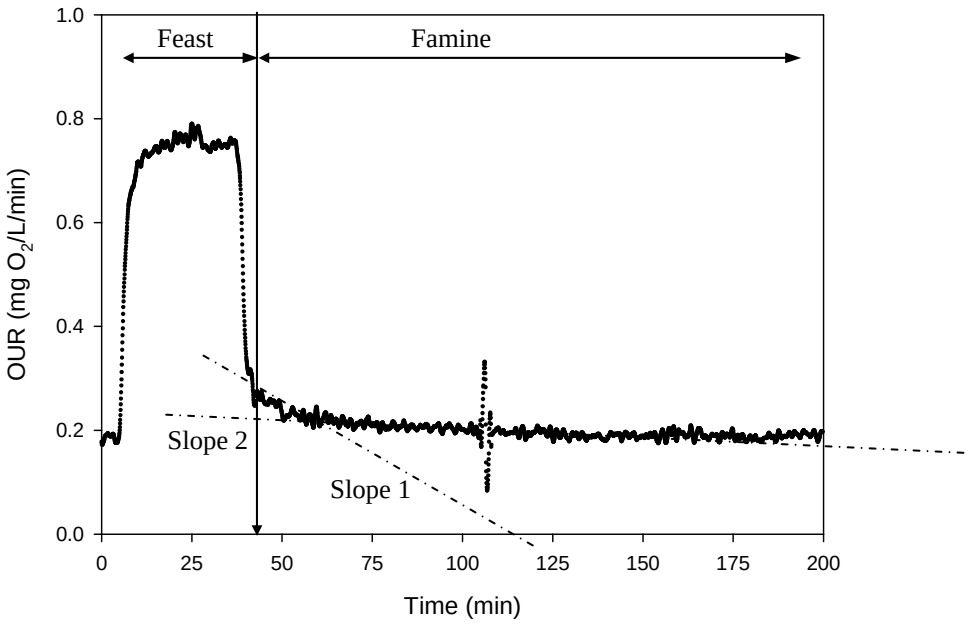

Figure V.C1 Oxygen uptake rate measurements from experiment V.C1.

Upon pulse addition of substrate (i.e. under the feast conditions), the OUR gradually increased to a maximum level following a fast transient period (*ca* 3-4 minutes). This transient period is frequently observed in OUR data obtained from batch experiments with pulse addition of substrate (Guisasola *et al.*, 2003 and Vanrolleghem *et al.*, 2004). The biomass activity continues at this maximum level until all external substrate is depleted for both storage and growth. When the external substrate was close to depletion the OUR dropped from the maximum to a level higher than the endogenous OUR. Endogenous OUR was measured prior to substrate addition. Under famine conditions, biomass grew using internal storage products, $X_{STO,}$ produced in the previous phase. As can be observed, the storage tail is not very important, indicating that the storage capacity of this biomass was not very high. The low storing capacity of the biomass strongly influenced the parameter estimation results obtained with this biomass.

Figure V.C1 also shows that two different slopes can be observed in the OUR obtained under famine conditions. This observation was the reason for the choice of second order kinetics for the description of the PHB degradation (see the model development Chapter V.B). The first slope corresponds to the area where the surface-saturation kinetics have more influence. Afterwards, the effect of the minimum PHB content is observed as the PHB content in the cell decreases and the PHB oxidation slows down. A similar pattern for acetate oxidation was observed in experiment V.C2 (Table V.C2).

Table V.C2 Experiment V.C2

EXPERIMENT V.C2	Respirometric batch experiment with biomass from Granollers WWTP
Equipment	LFS respirometer (V_0 = 1 L)
pH	7.5
Temperature	25 ºC
Pulses	50 mg COD (as acetate) -> 50 mg COD/L

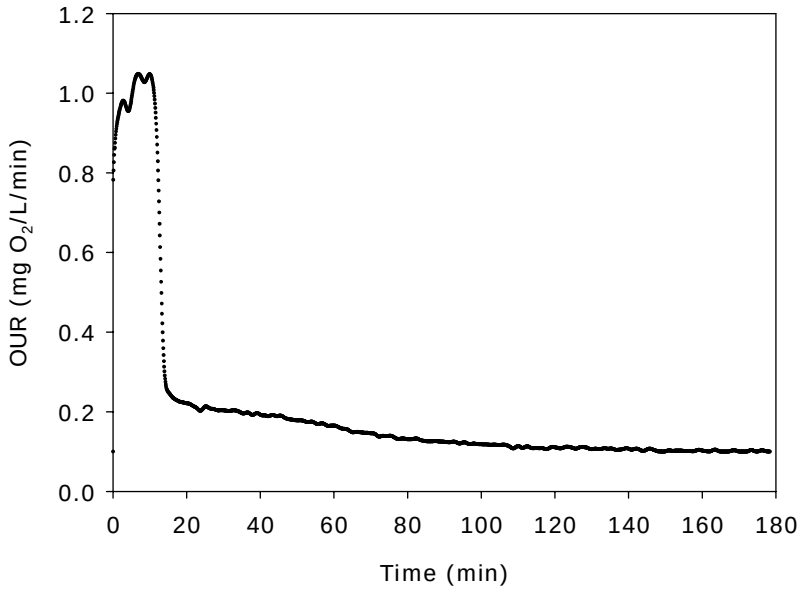

Figure V.C2 Oxygen uptake rate measurements from experiment V.C2.

It can be argued that ammonia and acetate measurements would be very helpful in this topic since acetate could indicate the switch between feast and famine phases and ammonia could be an indirect measurement of the biomass growth process. Ideally, the more measurements, the better in view of model building, validation and identification purposes. However, from a practical point of view, practical issues (e.g. sample volume, lack of required equipments, lack of required accuracy, etc.) may lead to minimise the number of measurements to the stricrly necessary.

The measurement of acetate would indicate when the substrate uptake is finished. However, this information can also be provided by the OUR profile, since a sharp drop is observed when acetate is fully depleted. Hence, acetate depletion can be indirectly monitored by the OUR shape. In some experiments, titrimetric data is also avaliable which is also an indirect monitorisation tool for acetate depletion.

Concerning ammonia measurements, they were not done for the experiments presented in this study for two main reasons. First, they are complicated to interpret due to residual ammonia released from decay processes. Second, in batch experiments with biomass performing simultaneous storage and growth there is usually negligible biomass growth due to low amount of substrate addition (low S/X ratio) and therefore there is negligible ammonia uptake. In the experiments presented in this study, the model simulated ammonia uptake was 1.5 mgN/L, which is difficult to be reliably detected. Figures V.C3 and V.C4 where the model fits are shown, also depict the simulated acetate and ammonia profiles.

V.C.3.2 PARAMETER ESTIMATION PROCEDURE

For the calibration of the model, the initial concentration of active biomass, $X_H(0)$, was necessary. As the biomass active fraction measurement is not straightforward, $X_H(0)$ is generally estimated using the baseline endogenous OUR level prior to substrate addition. According to the stoichiometry of the process the value of the endogenous OUR corresponds to equation V.C3:

$$OUR_{END}(0) = (1 - f_{XI}) \cdot b_H \cdot \frac{S_O}{S_O + K_O} X_H(0) + b_{STO} \cdot \frac{S_O}{S_O + K_O} X_{STO}(0) \qquad (V.C3)$$

As the biomass was left for an overnight aeration, the value of the initial storage product content ($X_{STO}(0)$) is very low when compared to $X_H(0)$. Hence, the contribution of the oxidation of storage products to the endogenous OUR value can be neglected (V.C4). For example, in experiment V.C3 (see below) the values of $X_{STO}(0)$ and $X_H(0)$ were 6.8 mg COD_{STO}/L and 800 mg COD_X/L respectively. The values of b_i, K_O and f_{XI} were fixed to the values mentioned in the ASM models (Henze *et al.*, 2000), i.e. 0.2 1/d, 0.2 mg O_2/L and 0.2 g COD/g COD, respectively.

$$OUR_{END}(0) = (1 - f_{XI}) \cdot b_H \cdot \frac{S_O}{S_O + K_O} X_H(0) \qquad (V.C4)$$

From a structural identifiability point of view, it is not possible to obtain unique values of both b_H and $X_H(0)$ using short-term (10 – 15 minutes) endogenous OUR measurements since there are an infinite number of solutions (parameter combinations of b_H and $X_H(0)$) to solve equation V.C4. This is because the decay of biomass is practically negligible within such short-period. Long-term (e.g. 10 days) monitoring of endogenous OUR is needed for unique estimation of b_H (Keesman *et al.*, 2000; Henze *et al.*, 2000; Ubisi *et al.*, 1997, Gabriel, 2000). Hence for given f_{XI} and b_H, the $X_H(0)$ can be calculated from the $OUR_{END}(0)$ data.

The estimation of the initial concentration of storage products, $X_{STO}(0)$, is really one of the most controversial issues when calibrating models with the storage process. If this value cannot be measured, its estimation using the OUR profile was observed to cause severe identification problems (results not shown), i.e. it had a too large confidence interval. Therefore, the initial concentration of storage products, $X_{STO}(0)$, was either measured (in experiments V.C2 and V.C3) or estimated (in experiment V.C1) using a step-wise procedure (Dochain and Vanrolleghem, 2001). In any case, as the biomass was subjected to famine conditions during hours before the experiment started similar, low (and close to the minimum) values are expected.

The maximum growth rate of biomass on X_{STO}, μ_{MAXSTO}, was assumed to be in the same order of magnitude as the maximum growth rate of biomass on external substrate, $\mu_{MAX,S}$, in order to keep the model calibration exercise at a reasonable complexity. It is important to note that from a parameter estimation point of view, any possible error involved in this assumption would be compensated by the estimate of K_2 or K_1. The yield coefficients for storage, (Y_{STO}), direct growth on S_S, ($Y_{H,S}$) and growth on X_{STO}, ($Y_{H,STO}$) were calibrated by estimating the δ parameter using the relations given in equations V.C5a-c adopted from van Aalst-van Leeuven *et al.* (1997). The maximum storage rate, k_{STO}, and the maximum growth rate of biomass, μ_{MAX}, were calculated from the estimates of the maximum substrate uptake rate, q_{MAX}, and the fraction of substrate used for storage f_{STO} according to the substrate flux model described in the previous chapter.

$$Y_{H,S} = \frac{4 \cdot \delta - 2}{4.2 \cdot \delta + 4.32} \cdot \frac{4.2}{4}\ ;\ Y_{STO} = \frac{4 \cdot \delta - 2}{4.5 \cdot \delta} \cdot \frac{4.5}{4} \text{ and } Y_{H,STO} = \frac{4.5 \cdot \delta - 0.5}{4.2 \cdot \delta + 4.32} \cdot \frac{4.2}{4.5} \qquad (V.C5a\text{-}c)$$

V.C.3.3 PARAMETER ESTIMATION RESULTS

Parameter estimation results obtained using OUR measurements with experiments V.C1 and V.C2 are summarised in Table V.C3, while best fits of the model to the experimental data are shown in Figures V.C3 and V.C4. As can be observed, the model fits are quite acceptable.

Table V.C3 Parameter estimation results with the simultaneous storage and growth model.

Parameters	Experiment V.C1	Confidence Interval*	Experiment V.C2	Confidence Interval**
Parameters estimated				
q_{MAX} (1/d)	1.67±0.09	5.4%	6.43±0.05*	0.78%
f_{STO} (g COD_S/g COD_S)	0.29±0.07	24%	0.65±0.09	13.8%
δ (mol/mol)	2.88±0.16	5.6%	2.57±0.22	8.6%
K_S (mg COD_X/L)	0.6±0.4	67%	0.67±0.11	16%
K_1 (g COD/g COD)	0.015±0.029	193%	0.053±0.041	77%
K_2 (g^2 COD/g^2 COD)	$1.7\cdot10^{-4}\pm3\cdot10^{-4}$	182%	$9.8\cdot10^{-4}\pm1\cdot10^{-3}$	102%
τ (min)	2.73±0.12	4.4%	0.51±0.05	10%
Parameters estimated using the step-wise procedure				
$X_{STO}(0)$ (g COD_{STO}/L)	0.99 (estimated)		6.8 (measured)	
Parameters assumed				
b_H (1/d)	0.2		0.2	
b_{STO} (1/d)	0.2		0.2	
f_{XI}(g COD/g COD)	0.2		0.2	
Parameters calculated				
$X_H(0)$ (mg COD_X/L)	1650		800	
$q_{MAX}\cdot X_H(0)$ (mg COD_X/L/d)	2755		5144	
$\mu_{MAX,S}$ (1/d)	0.72		1.3	
k_{STO} (1/d)	0.4		3.31	
$\mu_{MAX,STO}$ (1/d)	0.72		1.3	
Y_{STO} (g COD_{STO}/g COD_{STO})	0.83		0.81	
$Y_{H,S}$ (g COD_X/g COD_S)	0.61		0.58	
$Y_{H,STO}$ (g COD_X/g COD_{STO})	0.71		0.68	

** Confidence intervals are presented in these columns as absolute relative percentage of the parameter estimates, i.e. (confidence interval/parameter)*100.

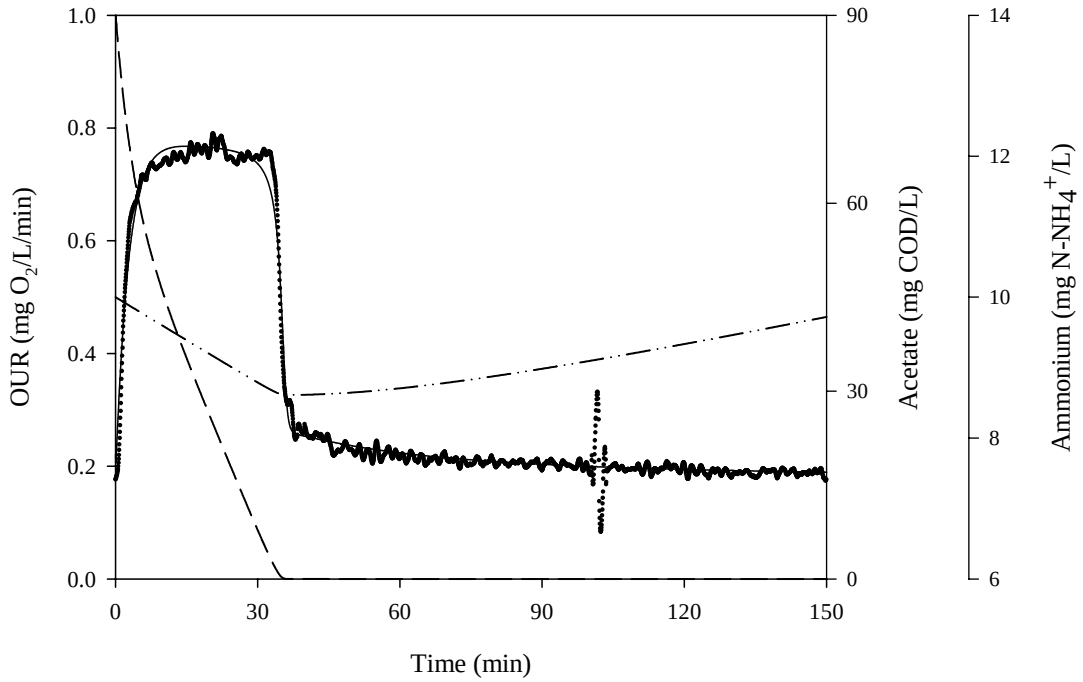

Figure V.C3 Model fits to the experiment V.C1. Experimental OUR (dotted), Simulated OUR (solid), simulated acetate (dashed), simulated ammonium (dash-dotted).

The ratio of substrate uptake to substrate used for storage, f_{STO}, was found low in experiment V.C1 compared to the value of experiment V.C2. As discussed in the previous chapter, the value of f_{STO} should theoretically be around 0.7 g COD/g COD for slow growing biomass adapted to their operational conditions, i.e. high SRT, (Beun *et al.*, 2001; van Loosdrecht and Heijnen, 2002). On the other hand, the storage fraction obtained in experiment V.C2 is in good agreement with this typical value. In any case, this value should not be taken as universal, since it is influenced by many factors such as the alternating feed pattern, the feed fractionation, etc,…. Some WWTPs may have low storing capacity biomass, though operated under SRT higher than 5.

The substrate uptake rate in experiment V.C1, i.e. $q_{MAX} \cdot X_H(0)$, is observed to be approximately half that of experiment V.C2. As a result, the kinetic parameters estimated in the first experiment were in general lower than the kinetic parameters estimated for the latter.

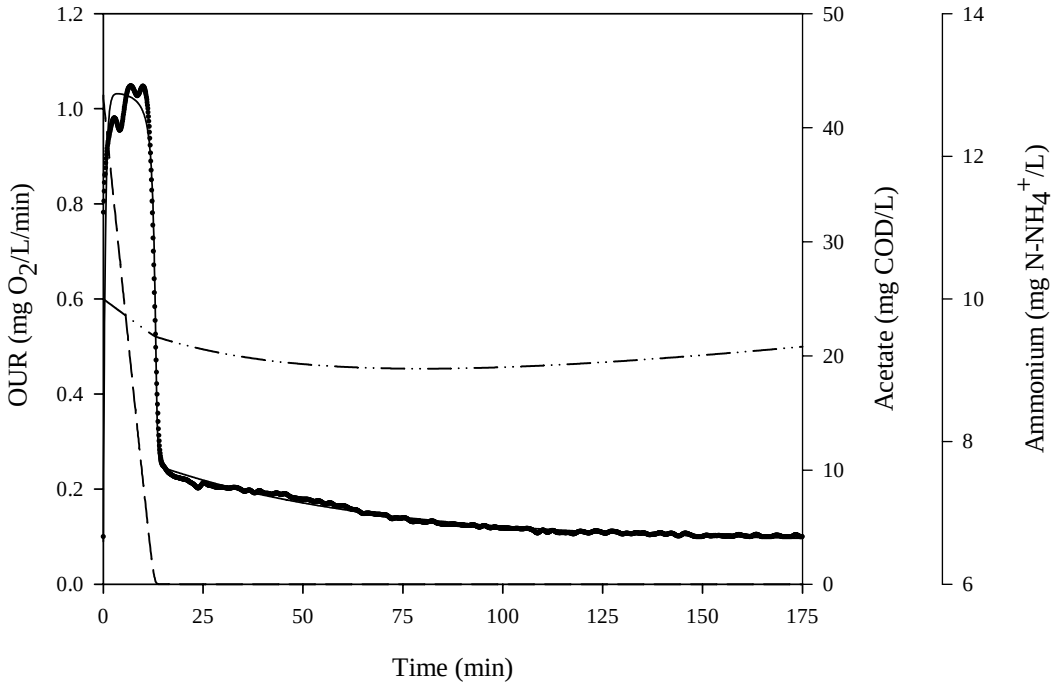

Figure V.C4 Model fits to the experiments V.C2. Experimental OUR (dotted), Simulated OUR (solid), simulated acetate (dashed), simulated ammonium (dash-dotted).

Nonetheless, the μ_{MAX} estimates of both biomass samples are noticeably lower than the typical range of values reported in literature for the maximum heterotrophic growth rate for municipal WWTPs (Henze *et al.*, 2000; Gernaey *et al.*, 2002b; Vanrolleghem *et al.*, 2004; etc.). The substrate affinity constants, K_S, of both experiments (Table V.B4) were also found to be in the same order of magnitude of the values obtained from other batch experiments (Gernaey *et al.*, 2002b; Vanrolleghem *et al.*, 2004). As can be observed the confidence interval obtained are very high and should be reduced. For this aim, a study on the practical identifiability of the parameters with OUR as a measured output was developed.

V.C.3.4 PRACTICAL PARAMETER IDENTIFIABILITY

Practical identifiability of a model structure is important as it tells which parameter combinations can be estimated under given measurement accuracy and quantity. In this way, one can improve the reliability and accuracy of the parameter estimation (Dochain and Vanrolleghem, 2001). For such identifiability study, output sensitivity functions of parameters and contour plots of the objective function were evaluated.

Output sensitivities of model parameters calculated using best-fit parameters obtained in experiment V.C2 are shown in Figure V.C5. The output sensitivity function of q_{MAX} is observed to be correlated with the output sensitivity function of f_{STO} and δ during the feast phase. However, in the famine phase these correlations are broken largely, thereby enabling to estimate those parameters simultaneously using OUR measurements. The sensitivity function of K_S also has a different trajectory than that of the sensitivity of q_{MAX} unlike what happens in pure-growth models where it is often the case that μ_{MAX} is correlated with K_S (Dochain and Vanrolleghem, 2001). Moreover, the output sensitivity functions of f_{STO} and δ are also almost perfectly correlated under the feast phase but again this correlation is broken during the famine phase, making these parameters uniquely identifiable as well.

The output sensitivity functions for K_1 and K_2 are observed to be correlated until a certain time instant beyond which the correlation is broken. In this regard, the length of the famine phase becomes very important for reliable estimation of these parameters. The output sensitivities of K_1 and K_2 have no specific correlation with the sensitivity functions of q_{MAX}, f_{STO} and δ respectively. This ensures reliable estimation of parameters K_1 and K_2 from the part of data collected under famine conditions.

In summary, the output sensitivity functions of the model parameters estimated in Table V.C3 suggest that they are practically identifiable using OUR measurements alone. These results are also supported with the analysis of the shape of the cost/objective function performed below.

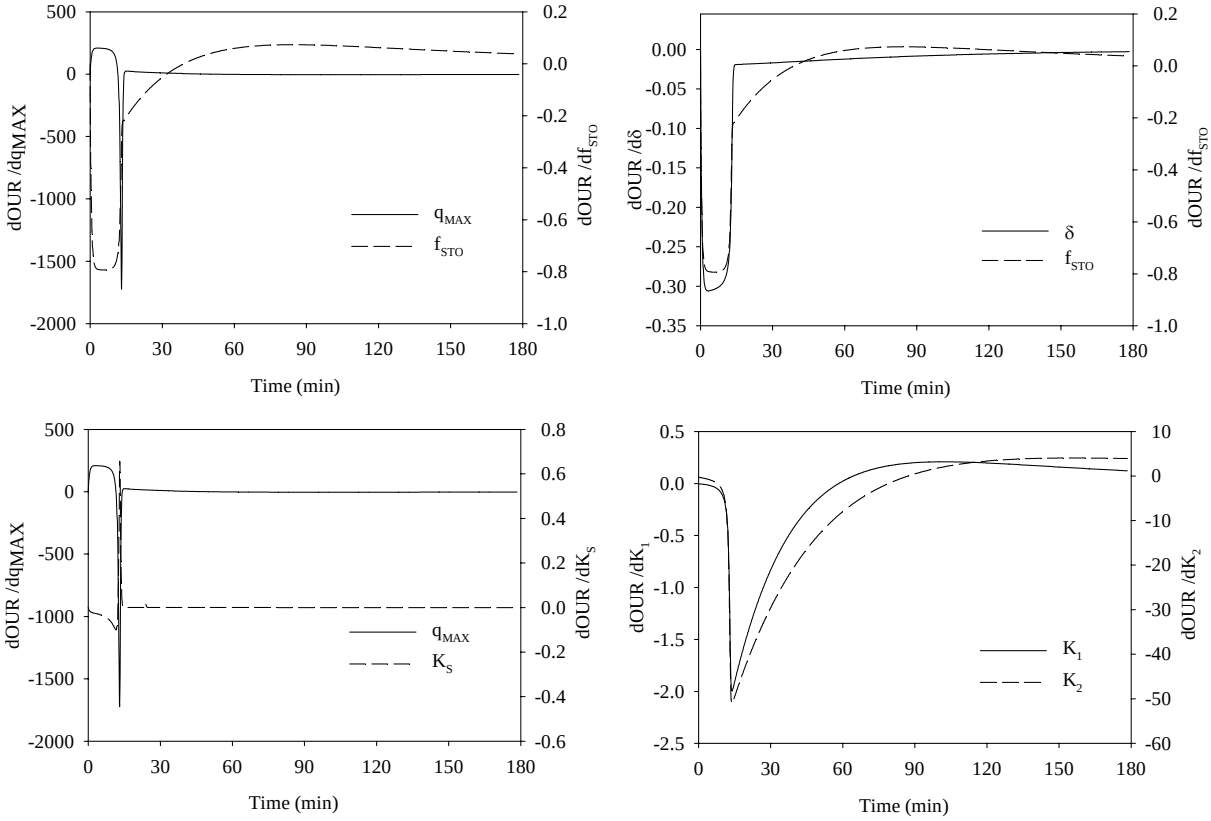

Figure V.C5 Output sensitivity functions of model parameters calculated around best-fit conditions for experiment B (see text for explanation).

The contour plots of the objective function (Figure V.C6) were calculated around the optimum for different combinations of parameters: f_{STO} and δ (Figure V.C5-left) and K_1 and K_2 (Figure V.C6-right).

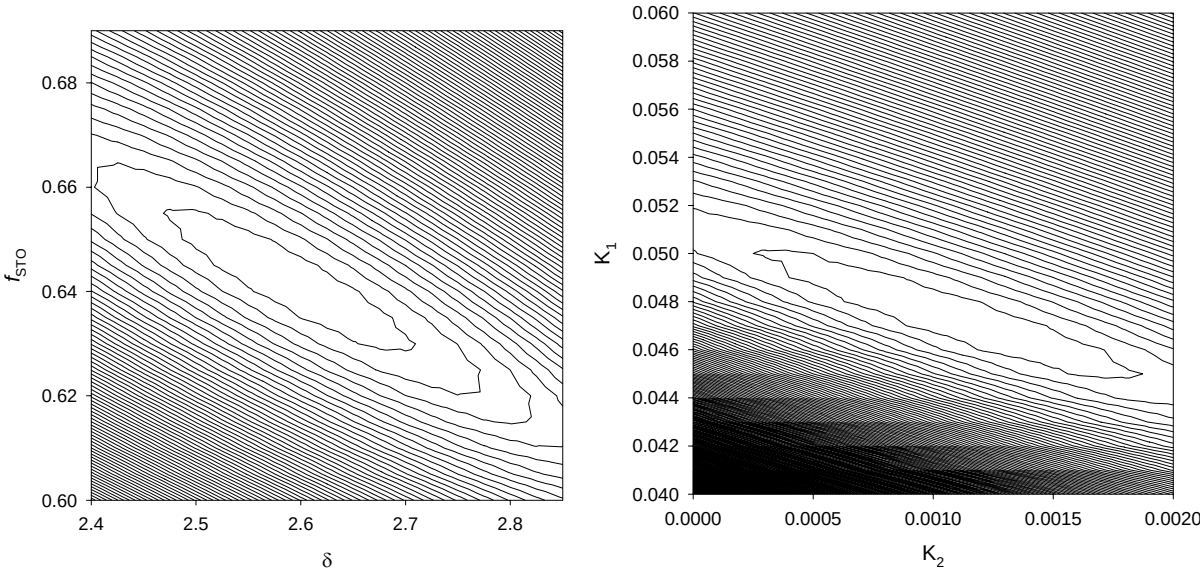

Figure V.C6 Contour plots of the objective functional used for parameter estimation as function of two parameters; f_{STO} and δ (LEFT) and K_1 and K_2 (RIGHT).

The contours of the objective function are large in both planes of the two-parameter subsets i.e. f_{STO} - δ plane and K_1 - K_2 planes respectively. Particularly in the plane K_1 and K_2 (right), the objective function is observed to be valley-like in a certain direction. This means that several combinations of parameters K_1 and K_2 will give almost equally good fits to the data leading to large confidence intervals of the parameter estimates (Baltes *et al.*, 1994; Dochain and Vanrolleghem, 2001). This is indeed observed in the parameter estimation results. The relative errors on parameter estimates K_1 and K_2 are calculated to be 77% and 102% respectively in experiment V.C2. When confronted with such situation, optimal experimental design (OED) has been shown to improve parameter estimation accuracy (Dochain and Vanrolleghem, 2001; Vanrolleghem *et al.*, 1995)

V.C.4 Optimal experimental design (OED)

V.C.4.1. SHORT OED DESCRIPTION

The OED procedure detailed in Dochain and Vanrolleghem (2001) has shown to be a very useful tool for model calibration purposes. Several works have used OED to improve/reduce the confidence intervals in parameter estimation (e.g. Petersen 2000; Baetens *et al.*, 2000 or Insel *et al.*, 2003, among many others). Next, the OED methodology is shortly described. a short description of this methodology. For an accurate description, the reader should be referred to Dochain and Vanrolleghem (2001).

As described in chapter IV, the parameter estimation procedure consists of the minimisation of a weighted sum (J) between model outputs (y) and the experimental measurements (y_M), with Q as weighting matrix.

$$J(\theta) = \sum_{i=1}^{N} \left(y(t_i, \theta) - y_m(t_i)\right)^T \cdot Q_i \cdot \left(y(t_i, \theta) - y_m(t_i)\right) \qquad \text{(V.C6)}$$

where θ represents a parameter of the model.

The effect of a small variation of a parameter on J around the optimum can be written as equation V.C7:

$$J(\theta_{OPT} + \partial\theta) = \sum_{i=1}^{N} \left(y(t_i, \theta_{OPT} + \partial\theta) - y_m(t_i)\right)^T \cdot Q_i \cdot \left(y(t_i, \theta_{OPT} + \partial\theta) - y_m(t_i)\right) \quad \text{(V.C7)}$$

Part of this equation can be simplified using the sensivity functions (Y_θ) [eq. V.C8]:

$$y(t, \theta_{OPT} + \partial\theta) \approx y(t_i, \theta_{OPT}) + \left[\frac{\partial y(t_i, \theta)}{\partial\theta}\right]_{\theta_{OPT}} \partial\theta = y(t_i, \theta_{OPT}) + Y_\theta(t_i, \theta)\partial\theta \quad \text{(V.C8)}$$

As a result, equation V.C9 is:

$$J(\theta_{OPT} + \partial\theta) = J(\theta_{OPT}) + \partial\theta^T \left(\sum_{i=1}^{N} Y_\theta(t, \theta_{OPT})^T \cdot Q_i \cdot Y_\theta\left(t_i, \theta_{OPT}\right)\right) \cdot \partial\theta \quad \text{(V.C9)}$$

According to the FIM definition (V.C1), equation V.C9 can be transformed to:

$$J(\theta_{OPT} + \partial\theta) = J(\theta_{OPT}) + \partial\theta^T FIM \cdot \partial\theta \quad \text{(V.C10)}$$

It is required that small variations on the parameter result in a high variation of the J value for a reliable parameter estimation. Hence, it is necessary that the second part of equation V.C10 (i.e. FIM) is maximised. The OED procedure aims to decide (by means of simulation) which of the potential experiments to be done will provide the maximum information. Several scalar functions of FIM can be used as a measure of the quality and quantity of the information provided by the FIM (Petersen, 2000; Hidalgo and Ayesa, 2001). A short description of the OED procedure sequence is:

1. Reference experiment: The model is precalibrated with a reference experiment. The parameter estimation values obtained in the reference experiment will be used for the posterior simulations. These values act as initial guess of the real parameter estimation values.

2. Experimental degrees of freedom: There should be some operational condition that could be changeable among experiments in order to have different potential experiments. This degree of freedom can be any: temperature, S/X ratio, volume, time pulse…. Obviously, the effect of a change on this operational condition should be described by the model.

3. Scenarios simulation: A wide range of the possible scenarios (i.e. different values of the degreee of freedom) are simulated using the parameters estimated in the reference experiment. The value of FIM is calculated in each simulation.

4. Once the FIM is calculated, the optimal experimental design (the one which contains more information) is chosen and implemented in reality. This experiment would contain the higher information and the lower correlation possible for a low parameter estimation error. There are several properties of the FIM matrix that are related to the amount of information contained and to the parameter correlation. This scalar properties are the basis of the criteria to decide which is the optimal experimental design (Dochain and Vanrolleghem, 2001; Hidalgo and Ayesa, 2001)

Criterion A: min tr(FIM^{-1}). Minimising the trace equivals to minimise the arithmetic average of the parameter errors (i.e. the squares of the lengths of the axis of the confidence ellipsoids). If the FIM is poorly conditioned, its inversion may lead to numerical problems. In this case, an alternative could be maximising the trace of the FIM itself (modA = max tr(FIM)).

Criterion D: max det (FIM). Maximising the determinant equivals to minimise the volume of the confidence region, and, hence to minimise the geometric average of the parameter errors.

Criterion E: max λ_{MIN}(FIM). Maximising the smallest eigenvalue equivals to minimise the length of largest axis of the confidence ellipsoid. Thus, the largest confidence interval is minimised. A modification of this criterion (modE) is minimising the ratio $\lambda_{MAX}/\lambda_{MIN}$(FIM) (= cond (FIM)). By minimising the condition of the FIM, it is aimed that the ratio of the λ_{MAX} and λ_{MIN} tends to 1. This is the minimum value of the ratio possible and would indicate that the confidence ellipsoid is an hypersphere, which means no parameter correlation.

V.C.4.2 OED FOR IMPROVING PARAMETER ESTIMATION

The OED sequence was utilised to improve the parameter estimation errors with experiment V.C2 as the reference experiment. The parameter subset considered for parameter estimation consisted of q_{MAX}, f_{STO}, K_1, K_2, τ, K_S and δ. The experimental degrees of freedom were chosen to be:

(1) single or two consecutive pulse additions of acetate
(2) amounts of first (and second) pulse additions
(3) time instant of the second pulse addition.

The duration of each experiment was fixed to 200 minutes. The substrate to biomass ratio, S/X, was constrained to 0.1 (g COD_S/g COD_X) in order to prevent any possible physiological change at the cellular level (Chudoba *et al*., 1992; Grady *et al*., 1996). Considering that the $X_H(0)$ was approximated as 800 mg COD_X/L, the total added substrate was fixed to 80 mgCOD/L.

An iterative OED procedure was followed. The FIM, which is the basis for OED, is calculated to summarise the information content of each hypothetical experiment under different combinations of the above-mentioned degrees of freedom (Dochain and Vanrolleghem, 2001). The D and Mod-E criteria of FIM, the most frequently used FIM properties, are also used in this study (Dochain and Vanrolleghem, 2001).

The results of OED under various combinations of degrees of freedom are summarised in Figures V.C7. The first pulse is added at time zero and the time of the second pulse is a degree of freedom. The objective is to find an experiment with the lowest Mod-E and the highest D criteria values. It can be seen from Figure V.C6 (see the circled regions) that the optimal experiment according to the OED analysis is a two pulse addition of (40 mg COD/L each) where the second pulse is added around 20 min, which corresponds to an addition just before the first pulse of substrate is completely taken up by the biomass. This is very similar to the results of Vanrolleghem *et al.* (1995). The optimal experiment resulted in two peaks in the OUR profile, because it improves the accuracy of parameter estimation of the feast phase. Moreover, the parameters of the famine phase are also better estimated thanks to the increased PHB content of the cell and the elongated OUR tail thanks to the previous two pulses.

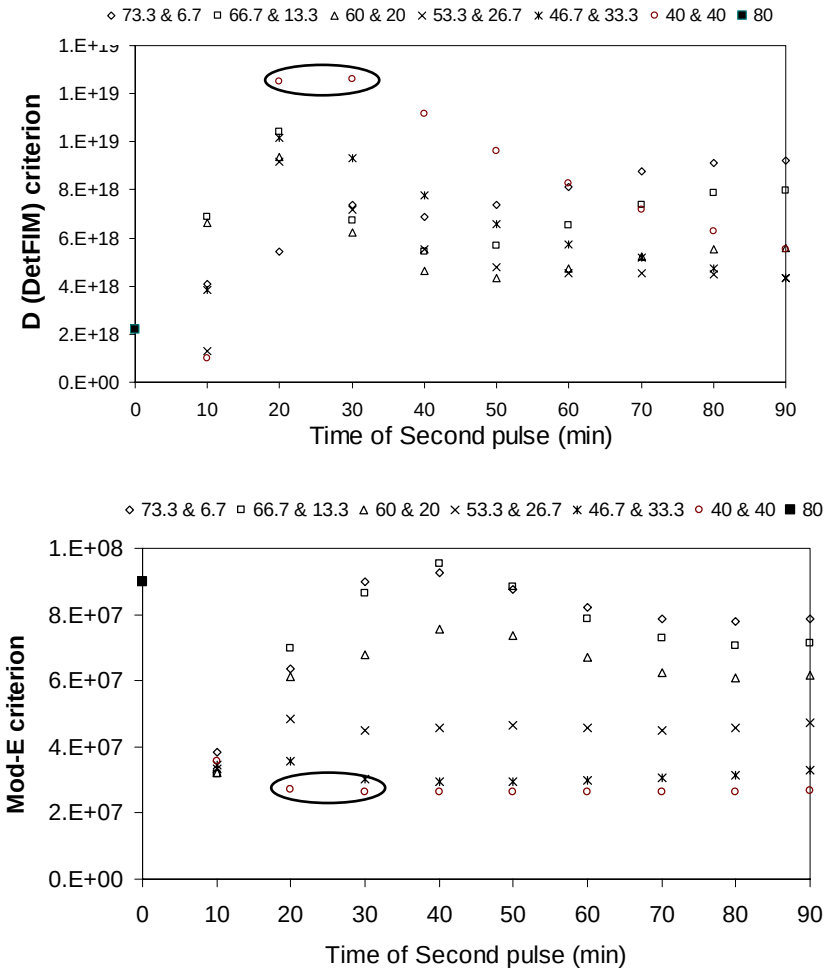

Figure V.C7 Properties of FIM as a function of the pulse time and the concentration of the pulses: D-criterion (top) and Mod-E criterion (down) (see text for explanation).

V.C.4.3 IMPLEMENTATION OF THE OED EXPERIMENT

Experiment V.C3 (Table V.C5) was the optimal experiment resulting from the OED study. This experiment was conducted using the same biomass as in experiment V.C2.

Table V.C5 Experiment V.C3

EXPERIMENT V.C3	OED experiment
Equipment	LFS respirometer (V_0 = 10 L)
pH	7.5
Temperature	25 ºC
Pulses	2·800 mg COD (as acetate) -> 80 mg COD/L

Figure V.C8 shows the experimental results including off-line PHB measurements. Upon the first pulse addition of acetate, the OUR immediately increased to a maximum level following a fast transient. Parallel to this increase in the OUR, the PHB content of the biomass also increased linearly in time. After the first pulse of acetate was depleted, the OUR dropped immediately. The same phenomenon as in the first acetate pulse was repeated in the second pulse addition of acetate. The formation of PHB was continued with a linear increase for as long as acetate was present. After the second pulse depletion, PHB started to decrease gradually following a non-linear pattern. Concomitantly, the OUR also decreased following a non-linear pattern due to the oxygen uptake for biomass growth on PHB.

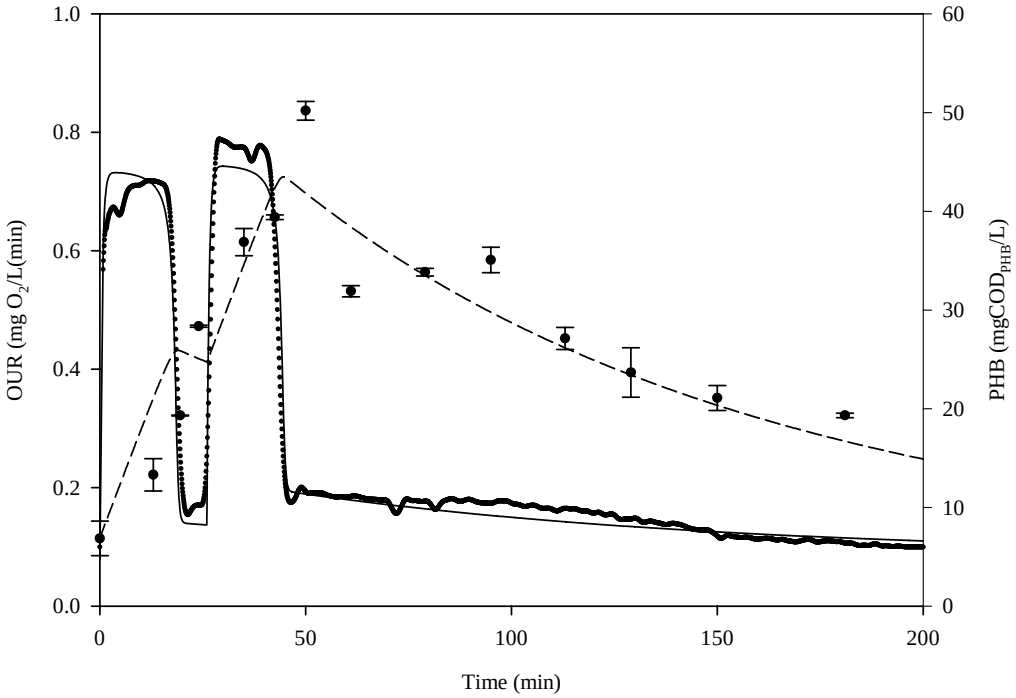

Figure V.C8 OED experiment; two pulse additions of equal amounts of acetate (40 mg COD/L). Experimental OUR (dotted) and PHB (circles) and modelled OUR (solid line) and PHB (dashed line)

The parameter estimation results for the OED experiment by only using OUR measurements are shown in Table V.C6. It is important to stress that the PHB measurements were not used for model calibration, but instead they were compared with the predictions of the model calibrated using OUR measurements alone. The model predictions for PHB were in agreement with the measured PHB content during the two consecutive pulse additions of acetate. Moreover, the model fit to the OUR measurements is acceptable. However, the model was unable to perfectly fit the second peak in the OUR profile as discussed in the next section.

Table V.C6. Parameter estimation results for the OED experiment using only OUR data.

Parameters	The OED experiment	Confidence interval*
	Parameters estimated	
q_{MAX} (1/d)	4.27±0.03	0.70%*
f_{STO} (g COD/g COD)	0.60±0.03	5.00%
δ (mol/mol ATP)	2.56±0.08	3.1%
K_S (mg COD/L)	0.70±0.1	14%
K_1 (g COD/g COD)	0.102±0.012	12%
K_2 (g COD/g COD)	$1.2 \cdot 10^{-3} \pm 3 \cdot 10^{-4}$	25%
τ (min)	0.51±0.07	14%
	Parameters measured	
$X_{STO}(0)$ (mg COD/L)	6.8	
	Parameters assumed	
b_H (1/d)	0.20	
b_{STO} (1/d)	0.20	
f_{XI} (mgCOD/mgCOD)	0.20	
	Parameters calculated	
$X_H(0)$ (mgCOD /L)	800.00	
$\mu_{MAX,S}$ (1/d)	0.97	
k_{STO} (1/d)	2.02	
$\mu_{MAX,STO}$ (1/d)	0.97	
Y_{STO} (g COD/g COD)	0.80	
$Y_{H,S}$ (g COD/g COD)	0.57	
$Y_{H,STO}$ (g COD/g COD)	0.68	

* Confidence intervals are presented in these columns as absolute relative percentage of the parameter estimates, i.e. (confidence interval/parameter)*100.

From a parameter estimation point of view, a remarkable improvement in parameter estimation accuracy was obtained from the OED experiment (comparing Table V.B4 and Table V.B6). Particularly the huge confidence intervals of K_1 and K_2 could be reduced from 77% and 102% to 12% and 25% respectively. In this regard, the application of the OED methodology for improving parameter estimation accuracy is clearly valuable.

Although the confidence intervals of the parameter estimates have been significantly reduced in the OED experiment, the parameter estimates themselves did not vary significantly compared to the values obtained in the reference experiment (i.e. experiment V.C2). For instance, the estimate of δ remained quite close to the value estimated in the reference experiment (Tables V.C4 and V.C6). However, the estimate of q_{MAX} was found lower than the value estimated in the reference experiment indicating that in the OED experiment biomass may have not yet reached its maximum substrate uptake rate. Since q_{MAX} was lower, the $\mu_{MAX,S}$, k_{STO} and $\mu_{MAX,STO}$ were also calculated to be lower compared to the reference experiment. A possible explanation for this observation could be physiological adaptation as discussed below.

Finally, it was observed experimentally that the amount of PHB formed per amount of acetate consumed, is equal to 0.54 g COD_{STO}/g COD_S, which is quite close to the previously estimated value (i.e. $Y_{STO} \cdot f_{STO}$) = 0.48. Moreover, both measured and estimated values fall in the range reported by Beun *et al.* (2001) for aerobic, slowly growing activated sludge cultures. This result supports the validity of the model as well as the calibration procedure using OUR measurements alone.

V.C.5 Discussion of the results

V.C.5.1. MODEL PERFORMANCE: PARAMETER ESTIMATION

The low estimates found for the maximum growth rate, $\mu_{MAX,}$ of both biomass samples are believed to be more realistic predictions of the true growth rate of activated sludge in municipal WWTPs, since the storage was properly accounted for in this study. Further, the estimated maximum substrate uptake rate of biomass is much higher than the amount used for the maximum growth rate of biomass which supports the hypothesis that activated sludge grows slower than what the substrate uptake rate allows (Beun *et al*., 2001; van Loosdrecht and Heijnen, 2002).

The efficiency of the oxidative phosphorylation, (δ), was found in the theoretically expected range i.e. 1 – 3 mol/mol (Beavis and Lehninger, 1986; Lehninger *et al.*, 1993; Beun *et al*., 2000) for experiments V.C1 and V.C2. Moreover, the yield coefficients calculated using the estimated δ were very similar even though different growth and storage kinetics were found between both experiments. This result supports the validity of the proposed model structure, which assumes that the macroscopic yield coefficients are independent of the growth rate, and can be estimated using a metabolic relation (see Chapter V.B).

The second order model adopted in this study to describe the utilisation of storage products under famine conditions fitted the OUR tail under famine conditions well. The parameter K_2, defined as the affinity of biomass as function of the storage content of biomass, X_{STO}/X_H, was found to be low for both experiments (V.C1 and V,C2). Moreover, the traditional affinity constant of biomass to storage products, K_{STO}, calculated as K_2/K_1 (see Chapter V.B), was found around 0.01 g COD/g COD which is in agreement with the value mentioned for PAOs in ASM2d (Henze *et al*., 2000). Moreover, Koch *et al.* (2000) estimated for K_{STO} a value of 0.1 g COD/g COD using the ASM3 model.

The estimated K_{STO} value in this study is significantly lower than the default value proposed for K_{STO} in ASM3 (1.0 mgCOD/mgCOD, Henze *et al.* (2000)). The high value of ASM3 is probably due to the severe parameter correlations of K_{STO} with the maximum growth rate of biomass (see chapter V.A).

The parameter K_1 defined as the regulation constant of biomass controlling the degradation of the storage product, was observed to change from one to another experiment, making it difficult to comment on. This variability is most probably due to the problems of practical identifiability encountered with the estimation of these two parameters K_2 and K_1 (see Figure V.C5). One way to improve the identifiability of this parameter is to apply an OED methodology, as done in this study for experiment V.C3, for all the rest of experiments. Another way of improving the identifiability of these parameters is naturally to use PHB measurements for parameter estimation on top of the OUR data. It is clear that further experiences are needed in this direction.

Direct biomass growth on substrate (acetate) can be compared with the biomass production based on internally stored PHB using the following ratio $(Y_{STO} \cdot Y_{H,STO})/Y_{H,S}$. This ratio is calculated to be close to 0.96 for both experiments, indicating that there is negligible reduction of the overall yield when PHB is used for growth, which is in agreement with the findings of Beun *et al*. (2000).

V.C.5.2 PRACTICAL IDENTIFIABILITY: OED EXPERIMENT

Estimation of $X_{STO}(0)$ was observed to cause severe parameter identification problems when OUR was used alone. To understand the reason of this difficulty, the objective function was calculated as a function of $f_{XSTO}(0)$ (i.e. the storage fraction of biomass expressed as $100 \cdot X_{STO}(0)/X_H(0)$), δ and f_{STO}. The contour plots of the objective function in both planes i.e. $f_{XSTO}(0)$- δ and $f_{XSTO}(0)$-f_{STO} are large and have a valley-like shape with a very flat bottom (Figure V.C9).

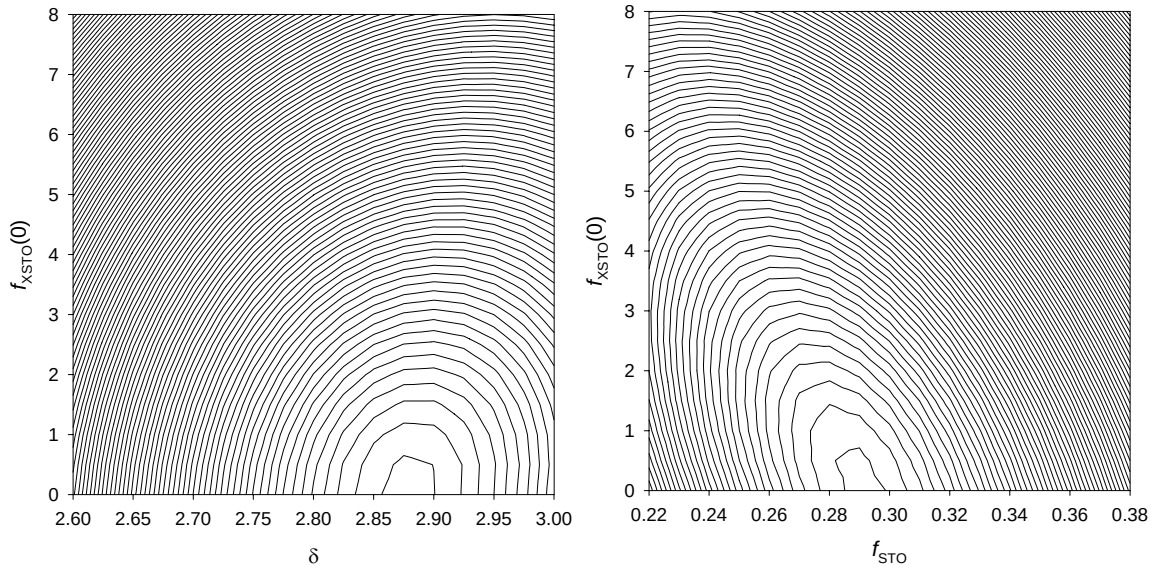

Figure V.C9. Contour plots of the objective function as a function of 2 parameters $f_{XSTO} - \delta$ (left) and $f_{XSTO} - f_{STO}$ (right).

This shape is known to cause severe problems to optimisation algorithms in finding the minimum (Dochain and Vanrolleghem, 2001). Moreover, large contour plots of the objective function indicate that there are many parameter combinations giving an almost equally good fit to the measurements. This implies that the confidence intervals of the parameter estimates would also be very large and the simultaneous estimation of parameters $f_{XSTO}(0)$ (and $X_{STO}(0)$), δ and f_{STO} would be very difficult.

To resolve this issue the $f_{XSTO}(0)$ should be fixed to either a measured value or by using step-wise parameter estimation (Dochain and Vanrolleghem, 2001). This step-wise parameter estimation procedure is already explained above. In the first step, $X_{STO}(0)$ was included in the parameters subset used in parameter estimation. Then, in the second step, the $X_{STO}(0)$ was eliminated from the parameters subset and the parameter estimation algorithm was performed again but this time the $X_{STO}(0)$ was fixed to the estimated value in the first step.

The application of the OED methodology was observed to provide remarkable improvements to the parameter estimation accuracy (Tables V.C4 and V.C6). For instance, it was possible to reduce the large confidence intervals of the parameters K_1 and K_2 from 77% and 102% to 12% and 25% respectively.

The model could not also describe the PHB data perfectly. However, it has to be considered that PHB measurements are difficult to perform and usually have a large standard deviation too (see Pratt et al., 2004). However, it is important to note that data do not contradict the proposed model. Indeed, the error bars included in the graph are calculated using the standard deviation of the triplicate measurements. Hence these error bars indicate the measurement error (which is low) and not the methodology error (which may be high).

In addition, the model could not perfectly describe the second peak in the OUR profile corresponding to the second acetate pulse (see Figure V.C8). Experiment V.C4 (Table V.C6) was developed to confirm that this increase in the double peak was not particular from experiment V.C3. The experiment was conducted in a different equipment (BIOSTAT B Fermenter) and with biomass withdrawn from a different WWTP (Tarragona, Catalonia, Spain). Figure V.C10 shows the experimental OUR profile obtained, where the second peak is clearly observed.

Table V.C6 Experiment V.C4

EXPERIMENT V.C4	Double peak experiment
Equipment	BIOSTAT B Fermenter (V_0 = 5.5 L)
pH	7.5
Temperature	25 ºC
Pulses	2·110 mg COD (as acetate) -> 20 mg COD/L

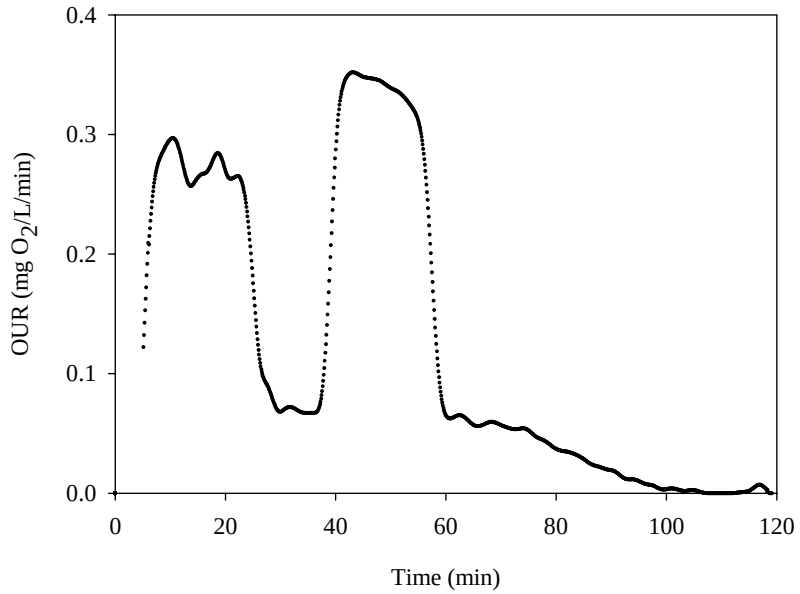

Figure V.C10 Exogenous OUR profile obtained in experiment V.C4

This discrepancy may be explained in two different ways. The first reason could be the physiological adaptation of the biomass. In other words, after the first pulse of acetate, the biomass increases its RNA and protein content and activity to sustain a higher growth rate (Vanrolleghem *et al*., 1998; van Loosdrecht and Heijnen, 2002; Lavallee *et al.*, 2005). In this respect, it is also important to note that parameter estimates with the OED experiment remained close to the ones of the reference experiment except q_{MAX}, which was found lower than the reference experiment. This supports the above-mentioned hypothesis that the biomass in the OED experiment undergoes a transient to increase its substrate uptake rate until it reaches the maximum substrate uptake, see e.g. the q_{MAX} obtained in the reference experiment. Similar phenomena were reported and discussed in detail in Vanrolleghem *et al*. (1998). Since the model developed in this study aims at modelling stable activated sludge cultures for WWTPs, the 10% increase in maximum OUR can be considered negligible in view of model calibration purposes.

An alternative explanation for this discrepancy could be that the growth on storage process was not inhibited by the external substrate concentration. This inhibition was included based on the experience of TUD. Moreover, it is logical that if biomass has external substrate available, it will put its efforts in substrate uptake (and direct growth on substrate) instead of using energy to grow on its storage product. In any case, experiment V.C3 was fitted again modifying the kinetics of the growth on storage product process from equation V.C11 to equation V.C12.

$$r_{GROWTH} = \mu_{MAX,STO} M_O M_{NH} \frac{\left(X_{STO}/X_H\right)^2}{K_2 + X_{STO}/X_H \cdot K_1} \cdot \frac{K_S}{S_S + K_S} X_H \qquad \text{(V.C11)}$$

$$r_{GROWTH,2} = \mu_{MAX,STO} M_O M_{NH} \frac{\left(X_{STO}/X_H\right)^2}{K_2 + X_{STO}/X_H \cdot K_1} \cdot \frac{K_{INH,S}}{S_S + K_{INH,S}} X_H \qquad \text{(V.C12)}$$

Hence, another parameter was added to the parameter estimation procedure. The results are shown on Table V.C7 and Figure V.C11.

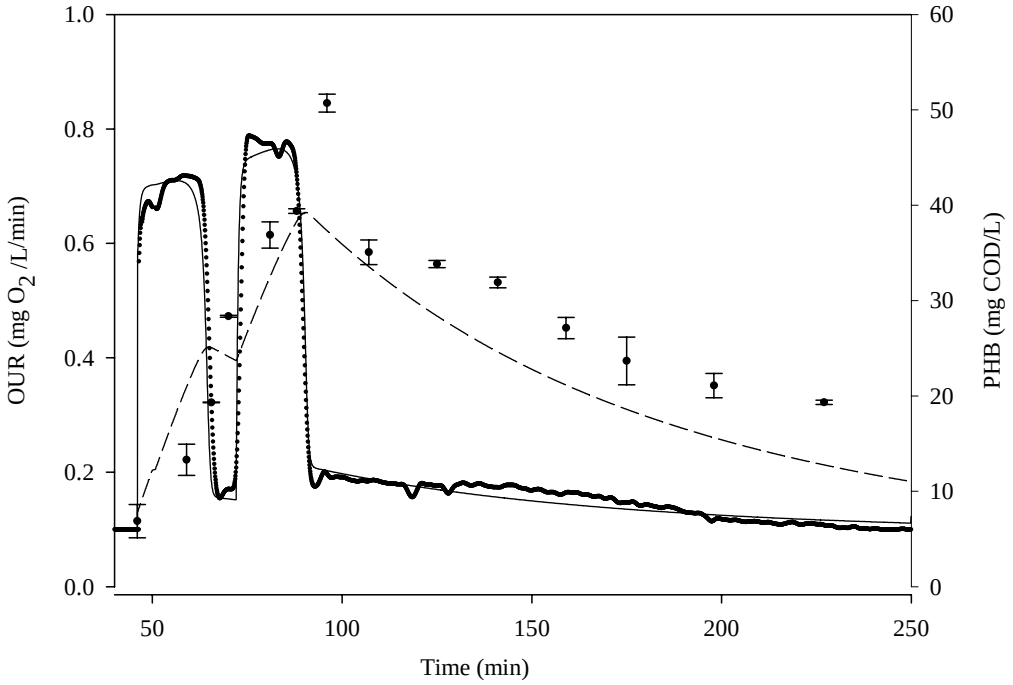

Figure V.C11 OED experiment; two pulse additions of equal amounts of acetate (40 mg COD/L). Experimental OUR (dotted) and PHB (circles) and modelled OUR (solid line) and PHB (dashed line)

As can be observed, the values obtained in both cases are not very different and the cost function has improved. Figure V.C11 show how the description of the second peak is accomplished with this kinetic modification. The value of $K_{INH,S}$ is very high (99.2), which indicates that this inhibiton is practically negligible in low-loaded experiments such as the OED experiment. This high value also questions whether growth on storage product is substrate inhibited. The most remarkable variation in the other parameters is on the δ value which has increased considreably from 2.56 to 2.82 and consequently, the yield values. With these values, the PHB production from acetate ($Y_{STO} \cdot f_{STO}$) is 0.515 which is closer to the 0.54 experimentally measured. The value of f_{STO} also increased from 0.6 to 0.63, and is closer to the value obtained in the reference experiment (0.65).

Table V.C7 Parameter estimation results for the OED experiment with modified kinetics of growth on storage products

Parameters	Former OED experiment	Modified kinetics
Parameters estimated		
q_{MAX} (1/d)	4.27	4.34
f_{STO} (g COD/g COD)	0.60	0.63
δ (mol/mol ATP)	2.56	2.82
K_S (mg COD/l)	0.70	0.92
K_1 (g COD/g COD)	0.102	0.0728
K_2 (g COD/g COD)	$1.2 \cdot 10^{-3}$	$1.1e^{-3}$
τ (min)	0.51	0.54
$K_{INH,S}$ (mg COD/l)	-	99.2
Parameters measured		
$X_{STO}(0)$ (mgCOD/l)	6.8	6.8
Parameters assumed		
b_H (1/d)	0.20	0.20
b_{STO} (1/d)	0.20	0.20
f_{XI} (g COD/g COD)	0.20	0.20
Parameters calculated		
$X_H(0)$ (mgCOD /L)	800.00	800.00
$\mu_{MAX,S}$ (1/d)	0.97	0.98
k_{STO} (1/d)	2.02	2.30
$\mu_{MAX,STO}$ (1/d)	0.97	0.98
Y_{STO} (g COD/g COD)	0.80	0.82
$Y_{H,S}$ (g COD/g COD)	0.57	0.60
$Y_{H,STO}$ (g COD/g COD)	0.68	0.70
COST FUNCTION (OUR)	1.43	1.27

On the other hand, Figure V.C11 shows the PHB prediction of the model using the parameters obtained with modified kinetics. Again, the PHB values are not accurately described and the model underestimates the real values. Although the kinetic modification proposed proposed above increases the accuracy of the model fits and it seems the parameters obtained are more realistic, further work is required on this field to establish the metabolic causes of this activity increase in the second peak.

Chapter V.C Conclusions

- In view of facilitating full-scale application of the model, a practical calibration procedure only requiring OUR data obtained from batch experiments was developed and applied successfully to calibrate the model. The predictions of the calibrated model were also confirmed by independent PHB measurements, supporting the validity of the model.

- OED methodology was shown to be valuable in view of improving the parameter estimation accuracy, particularly for the identification of the second- order model developed in this study.

- The maximum growth rate of heterotrophs was estimated to be between 0.7 – 1.3 d^{-1} for the sludge tested which is quite lower compared to the values reported in literature for the ASM models.

- The estimated yield coefficient for heterotrophic growth on acetate was around 0.58 g COD/g COD, lower than the values reported in literature for ASM models. It is believed that the proposed model gives a better prediction of the growth yield and the maximum growth rate of biomass in full-scale WWTPs since it accounts for the storage phenomenon. Finally, the estimated maximum substrate uptake rate of the biomass was much higher than the substrate usage rate at the maximum growth rate of the biomass.

- Finally, the model could describe the fact that the second peak is higher than the first if the growth on storage process was not inhibited by the external substrate concentration. However, this discrepancy may be due to the not modelled physiological adaptation of the biomass. In any case, further work on this topic is required.

CHAPTER V.D

Upgrading the biological COD removal model with titrimetric data

ABSTRACT

This chapter examines the link between titrimetric data and the biological COD removal process. According to the model described in Chapter V.B, the titrimetric data should be influenced by substrate uptake, CO_2 stripping and ammonia uptake for growth and release in the endogenous processes. The results show that titrimetry is a better tool for detecting the substrate depletion point than OUR and, in addition, they provide complementary information to the OUR measurement. An approximation of the total acid added for each mole of substrate taken up shows that titrimetry can also be used for substrate quantification. Finally, it is shown that if the model when calibrated with OUR and HP measurements provides a good description of the experimental profiles and decreases the confidence interval values with respect to the calibration with only OUR.

V.D.1 Introduction

Chapter V.B describes the model development for the biological COD removal process. This model was thought to be calibrated with both respirometric and titrimetric data. Titrimetric data (i.e. acid/base dosage necessary to maintain the pH constant) has already been used in previous models of biological COD removal (Gernaey *et al.,* 2002a,b; Sin, 2004; Pratt *et al.,* 2004). As detailed in Chapter V.B, three processes are the major influences on titrimetric measurements for COD removal:

1. The substrate uptake process requires acid dosage since a mole of proton is necessary to take up a mole of dissociated acid. Most of the acid is in dissociated form at pH close to neutrality.

2. The ammonia uptake process for growth requires base dosage since a mole of proton is released to the media to take up a mole of NH_3. Most of the ammoniac nitrogen is in NH_4^+ form at pH close to neutrality.

3. The CO_2 stripping process requires acid dosage to balance the CO_2 stripped from the gas to the liquid since most of the inorganic carbon is in bicarbonate form.

Figure V.D1 is an scheme of the link between the COD removal process and the titrimetric data, considering the substrate (HA) as a VFA. It is assumed that all the compounds go across the membrane in the non-disscicated form.

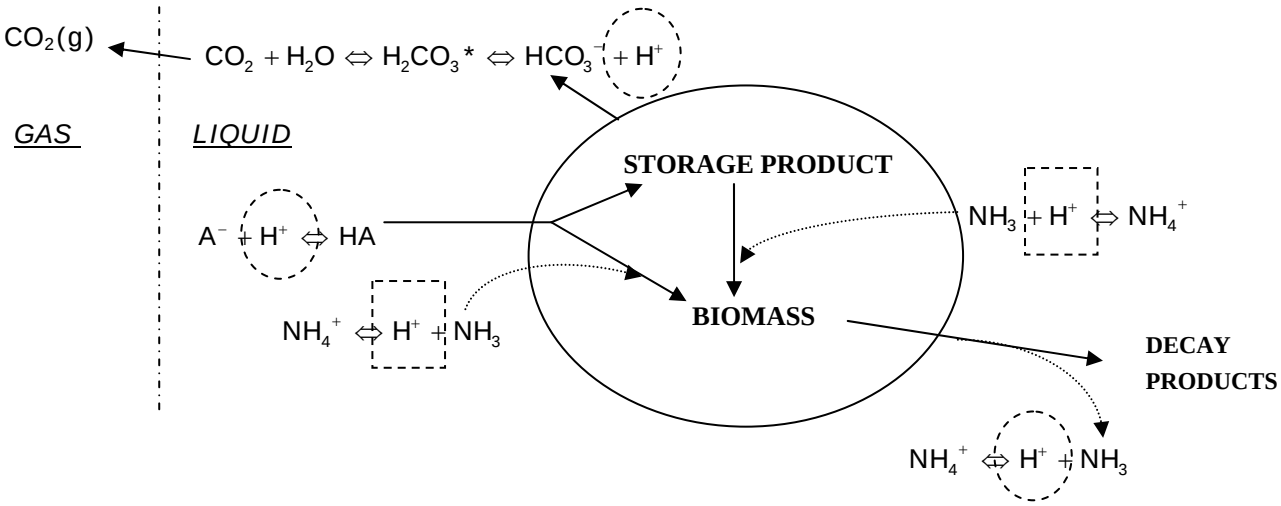

Figure V.D1 Link between cell activity and titrimetry for biological COD removal. Proton-consuming processes (circle). Proton-producing processes (square).

V.D.2 Respirometric-titrimetric batch experiments

V.D.2.1 Low storing capacity biomass

Several experiments were conducted to assess the behaviour of titrimetric measurements when a pulse of COD substrate is added. These experiments were performed in the LFS respirometer described in Chapter III.1.1, except for the ones performed in Belgium in the hybrid respirometer described in Chapter III.1.5. Respirometric-titrimetric experiments were performed with biomass withdrawn from different WWTP, which were operated under different conditions. Experiment V.D1 (Table V.D1) utilised biomass from Orrius WWTP, which only performs COD removal with a rather low SRT (around 4 days).

Table V.D1 Experiment V.D1

EXPERIMENT V.D1	Titrimetry with low storing capacity biomass
Equipment	LFS respirometer (V_0=0.90 L)
pH	7.5
Temperature	25 ºC
Acid used	HCl (1 M)
Pulses	33.1 mg COD (as acetate) -> 36.8 mg COD/L

Figure V.D2 shows the experimental profiles from experiment V.D1. The OUR profile plotted only corresponds to the exogenous OUR.

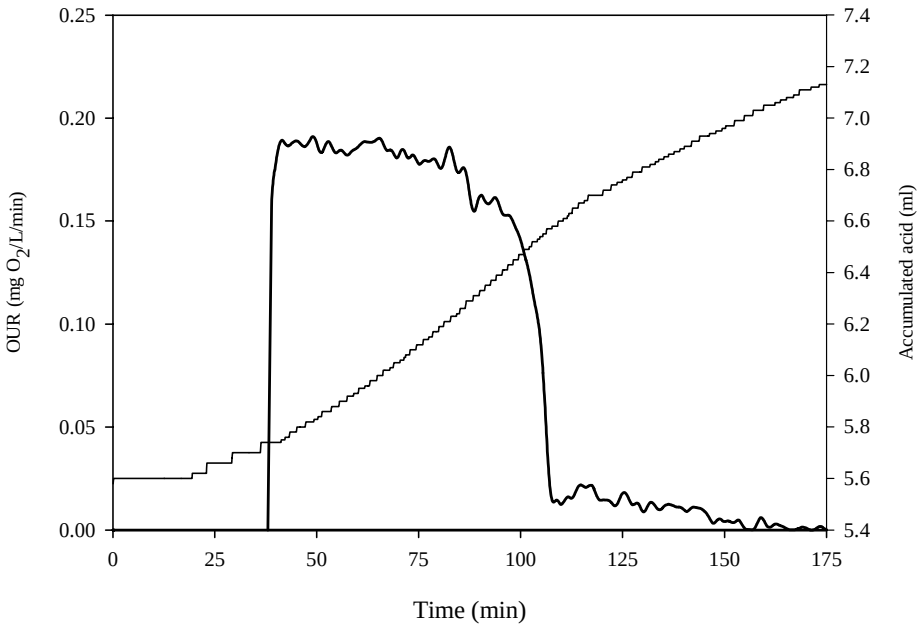

Figure V.D2 Respirometric-titrimetric profiles of experiment V.C5.

As can be observed, the acid dosage rate was very low before the pulse addition, probably because the amount of initial inorganic carbon was very low (no extra bicarbonate pulse was added). Once the pulse of acetate was added, the acid dosage rate increased whereas substrate was taken up. The biomass used in this experiment had a low storing capacity and the period with high acid dosage rate practically coincides with the OUR. Once the substrate was depleted, the acid dosage rate also decreased and was only influenced by CO_2 stripping.

The total amount of oxygen consumed in this pulse (calculated as the area under the exogenous OUR profile) is 12.8 mg O_2. The biomass growth yield (Y_H) can be approximated using equation V.D1.

$$Y_H = \frac{COD_{DEG} - \int_{t=1}^{t=tf} OUR(t)\cdot dt}{COD_{DEG}} = 1 - \frac{OC}{COD_{DEG}} \left[\frac{g\,COD_X}{g\,COD_S} \right] \qquad (V.D1)$$

where OC = oxygen consumed (mg O_2/L)
COD_{DEG} = amount of COD degraded

This is an approximate yield calculation because one single respirometric experiment may results in an erroneous yield value because small deviations in the oxygen consumption calculation would result in different yield values. This analysis is detailed in Chapter VI.B for the autotrophic yield estimation. Several respirometric experiments with different initial loads are needed for a reliable yield calculation.

In any case, if all the COD added is considered to be degraded, an approximate biomass yield of 0.61 g COD_X/g COD_S is obtained in experiment V.D1. This is a value which is smaller than the yield proposed for ASM1 (0.67) for biomass with low storing capacity. However, values in this range or even lower have been described for real sludge with acetate as carbon source (van Loosdrecht and Heijnen, 2002).

On the other hand, if the acid dosage due to the stripping is subtracted from the total accumulated acid (see Figure V.D3), the amount of acid added is approximately 0.48 ml, which means 0.48 mol H^+ added extra to the stripping. Theoretically, the amount of acid added should be close to the moles of sodium acetate added to the system, i.e. 0.57.

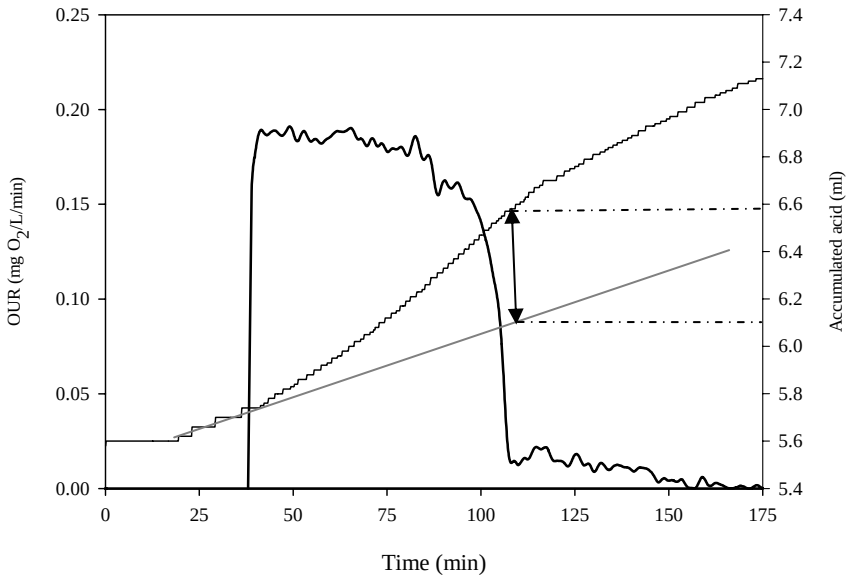

Figure V.D3 Approximation on the amount of acid required for acetate uptake

V.D.2.2 High storing capacity biomass

Experiment V.D2 (Table V.D2) was conducted using biomass from Granollers WWTP, which showed higher storing capacity. Figure V.D4 shows the experimental profiles of experiment V.D2. HPR was calculated to be compared with OUR. As described in Chapter I, HP is calculated as equation V.D2 and HPR is the first derivative of HP.

$$HP = \frac{V_{BASE} \cdot C_{BASE} - V_{ACID} \cdot C_{ACID}}{V_R} \quad [\text{mol eq/L}] \qquad \text{(V.D2)}$$

where V_{ACID}/V_{BASE} = Accumulated volume of acid/base (ml)
C_{ACID}/C_{BASE} = Acid/base concentration (mol/ml)
V_R = reactor volume (L)

Table V.D2 Experiment V.D2

EXPERIMENT V.D2	Link between HPR and OUR
Equipment	LFS respirometer (V_0=0.90 L)
pH	7.5
Temperature	25 ºC
Acid used	HCl (1 M)
Pulses	33.1 mg COD (as acetate) -> 36.8 mg COD/L
	55.2 mg COD (as acetate) -> 61.3 mg COD/L
	88.3 mg COD (as acetate) -> 98.1 mg COD/L

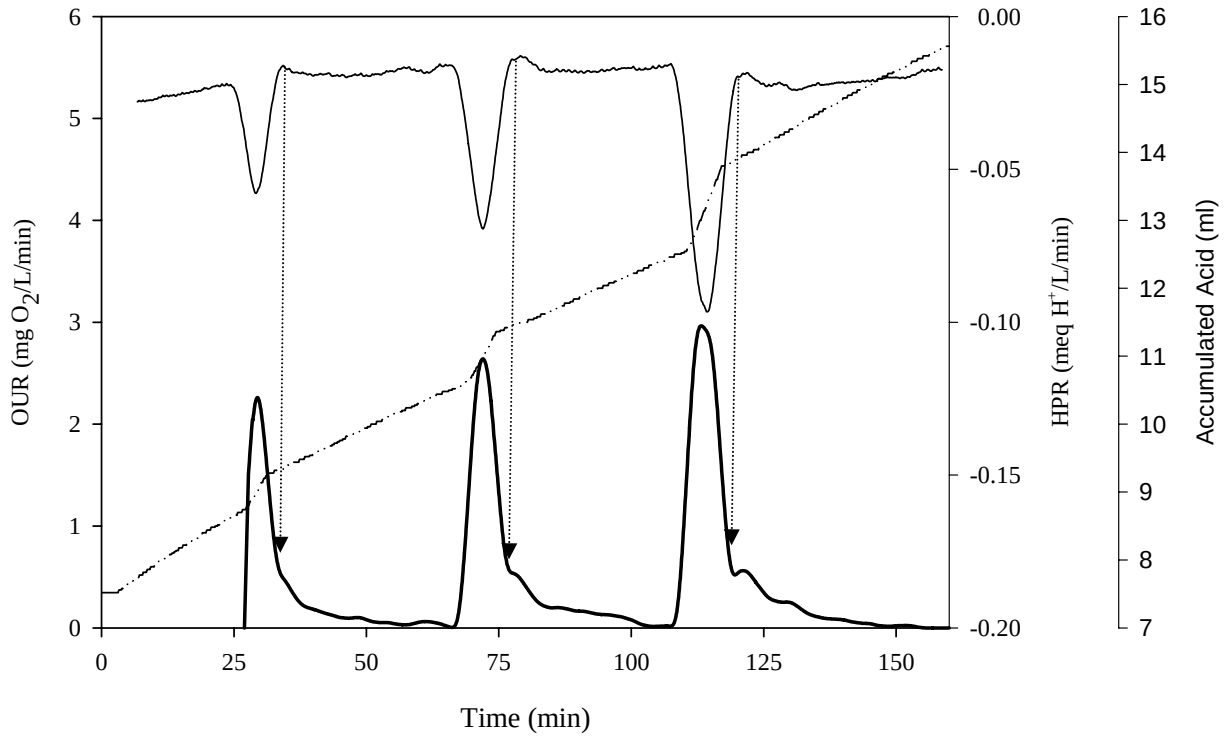

Figure V.D4 Respirometric-titrimetric profiles of experiment V.C6. Exogenous OUR (thick line), HPR (thin line) and acid dosage (dashed line)

As can be observed, when the pulse of substrate is added acid dosage rate increases and HPR decreases because protons are consumed faster to maintain the pH at 7.5. Nevertheless, HPR is only proportional to OUR in the first part of the pulse. Theoretically, this should be the period with substrate in the medium. After substrate depletion, there is some oxygen consumption due to the growth on storage product but HPR remains constant because there is no substrate uptake. In this period, HPR is only caused by ammonia uptake for growth (which is practically negligible) and CO_2 stripping.

In addition, the value of HPR before and after the second and third pulses is constant. In these cases, the constant BPPR hypothesis of Gernaey *et al.,* (2002a) could be successfully used.

The main conclusion of this experiment is that titrimetry (i.e. HP or HPR) is a successful tool to monitor the substrate (VFA) presence in a bioreactor. The substrate depletion point can be detected in a simpler way than with OUR because of the oxygen consumption due to growth on the storage product after substrate depletion. In this experiment, the amount of acid added was also compared to the amount of substrate added, and the results are shown on Table V.D3.

Table V.D3 Comparison of acid added with substrate added in experiment V.D2

Pulse	$NaCH_3COO$ (moles)	H^+ added (moles)	H^+/NaAc
1	0.57	0.35	0.61
2	0.95	0.56	0.59
3	1.52	1.00	0.66

As can be observed, the ratio of acid added to substrate added is lower than one (which should be the theoretical one). The reasons for such a low values are not very clear to the authors. It may be that the cell take up part of the acetate on dissociated form and maintain the cell electroneutrality taking up a cation different than a proton. In any case, further work on this topic is needed with more experiments at different pH values. However, it should be noted that the obtained ratios are very similar among them. The differences among the ratios are probably caused by the non-automated empirical method used for the calculation of the acid added (i.e. subtracting the stripping contribution from the real one).

In this sense, experiments V.D3 (Table V.D4) were conducted to assess the effect of using a substrate different from a VFA. In this case, ethanol and methanol were chosen. The biomass of this experiment was withdrawn from Maria Middlelares WWTP (Belgium). Figure V.D5 shows the experimental profiles of experiment V.D3.

Table V.D4 Experiments V.D3

EXPERIMENT V.D3	Respirometric-titrimetric measurements with non-VFA substrates
Equipment	Hybrid respirometer (V_0=3.2L)
pH	8
Temperature	25 ºC
Acid used	HCl (0.5 M)
Pulses	50 mg COD (as methanol) -> 15.6 mg COD/L
	100 mg COD (as ethanol) -> 31.28 mg COD/L

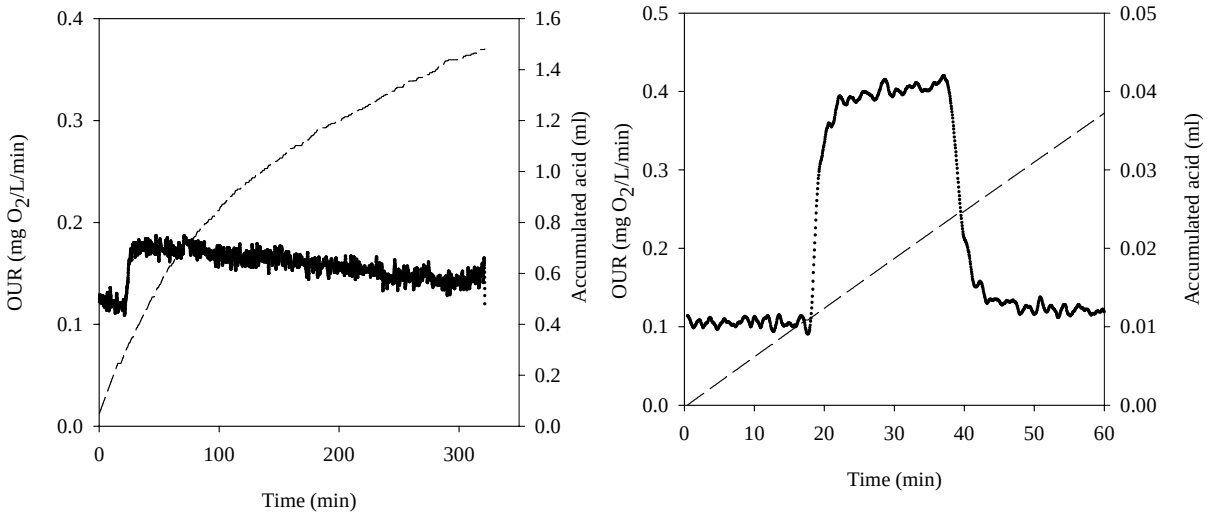

Figure V.D5 Respirometric-titrimetric profiles of experiment V.D3. Methanol as substrate (LEFT) and ethanol as substrate (RIGHT). OUR (dotted and acid dosage (dashed).

Theoretically, the acid dosage rate should not be influenced by the uptake of these substrates because they are not dissociated. As can be observed, the experimental results are in agreement with this idea. In the experiment with methanol, the acid dosage profile is the typical profile obtained with only CO_2 stripping, where the bicarbonate concentration is close to steady state. On the other hand, the acid dosage profile is a typical line of constant CO_2 stripping.

V.D.3 Modelling of respirometric-titrimetric profiles

V.D.3.1 ESTIMATION OF THE Q_K MATRIX

The procedure used in this thesis for the parameter estimation error assessment is based on the Fisher Information Matrix (FIM), as detailed in Chapter IV. If Q_K is the covariance matrix of the measurement noise, the FIM is defined as equation V.D3.

$$FIM = \sum_{k=1}^{N} Y_{\theta}^{T}(k) Q_K Y_{\theta}(k) \qquad (V.D3)$$

where Y_θ stands for the so called output sensitivity function, which are a numerical approach to the derivate of the output variable with respect to one parameter.

Chapter VI.E details the estimation of the measurement error weighting matrix (Q_K) assessment for the experimental inputs used with two different equipments: LFS respiroemter and BIOSTAT B fermenter. Q_K was estimated following the method described in Petersen (2000), which uses data from a period where the value of the output variable was perfectly known. If possible, a period with constant variables was preferred. Q_K is usually chosen as the inverse of the measurement error covariance matrix (s^2), and it is a square matrix with the same number of files and columns as output measurements.

For example, Q_{OUR} was estimated before the pulse of substrate was added (i.e. endogenous respiration phase) in which OUR was supposed to be constant. The average of the data and the resulting residuals were calculated in this period of constant OUR. Figure V.D6-left shows the endogenous period used for Q_{OUR} estimation in the LFS respirometer. On the other hand, HPR is only constant for a certain period of time under well-defined conditions (i.e. high carbon dioxide concentration and low k_La_{CO2}). The experimental data used for Q_{HPR} estimation was collected just after the addition of Na_2CO_3 to the system, so that the conditions were the closer possible to the mentioned conditions when HPR should be constant. Figure V.D6-right shows the HPR period used for Q_{HPR} estimation in the LFS respirometer. The calculated s^2 for OUR was 2.307e-^{5} and 5.778e^{-6} for HPR (see Chapter VI.E for further information).

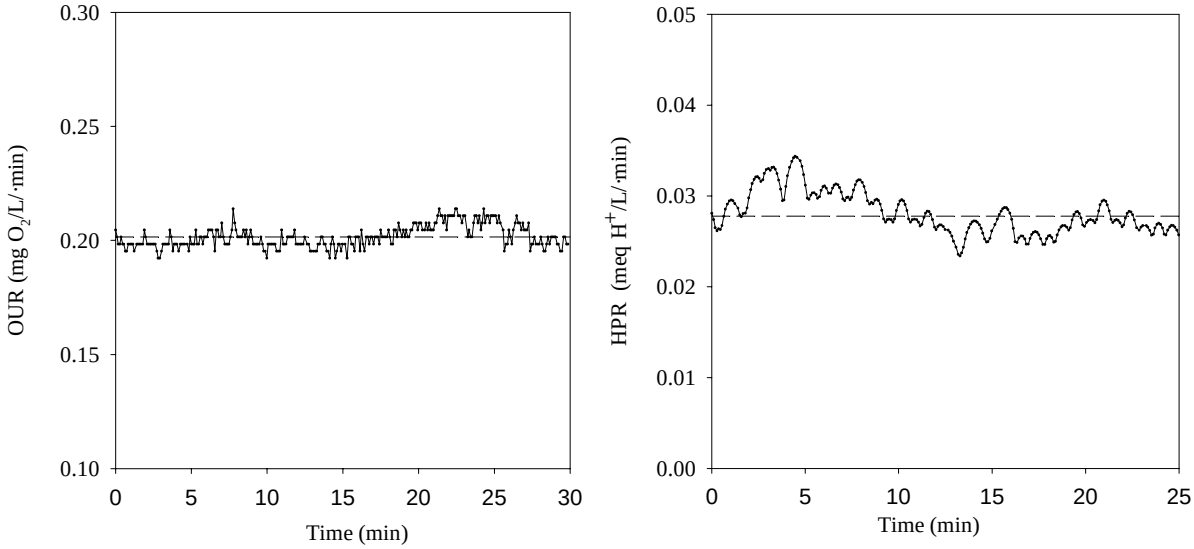

Figure V.D6 Q_{OUR} (LEFT) and Q_{HPR} (RIGhT) estimation in the LFS respirometer. Experimental value (solid); Mean (dashed)

V.D.3.2 PARAMETER ESTIMATION VALUES

The parameter estimation procedure followed in this section is the same as the one described in the previous chapter except for the titrimetric measurements. Two extra parameters have to be estimated for an accurate description of the titrimetric data: the initial concentration of the total inorganic carbon (TIC) and the equilibrium carbonic acid constant (pK1). Although, pK1 is a constant for pure water (6.36), this value should be estimated because it is highly influenced by the ionic strength of the medium. The higher the ionic strength, the lower the pK1. In addition, small deviations in this value result in large changes in the estimated titrimetric profile. The identifiability of these parameters with titrimetric data is deeply discussed in the next chapter for biological nitrogen oxidation (see Chapter VI.B).

Experiment V.D4 and V.D5 (Table V.D5) show typical respirometric-titrimetric OUR profiles from different WWTP. The biomass used in experiment V.D4 was withdrawn from Granollers WWTP (nitrification + biological COD removal). The biomass used in experiment V.D5 was withdrawn from Manresa WWTP where nitrification-denitrification is performed together with biological COD removal. In both cases, a significant storage effect can be observed.

Table V.D5 Experiments V.D4

EXPERIMENT V.D4	Modelling respirometric-titrimetric experiments: Granollers WWTP
Equipment	LFS respirometer (V_0=0.95 L)
pH	7.5
Temperature	25 ºC
Acid used	HCl (1 M)
Pulses	88.3 mg COD (as acetate) -> 93 mg COD/L (V.D4)

Table V.D6 Experiments V.D5

EXPERIMENT V.D4	Modelling respirometric-titrimetric experiments: Manresa WWTP
Equipment	LFS respirometer (V_0=0.95 L)
pH	7.5
Temperature	25 ºC
Acid used	HCl (1 M)
Pulses	55.3 mg COD (as acetate) -> 58 mg COD/L (V.D5)

Figure V.D7 compares the model fits with the experimental profiles.

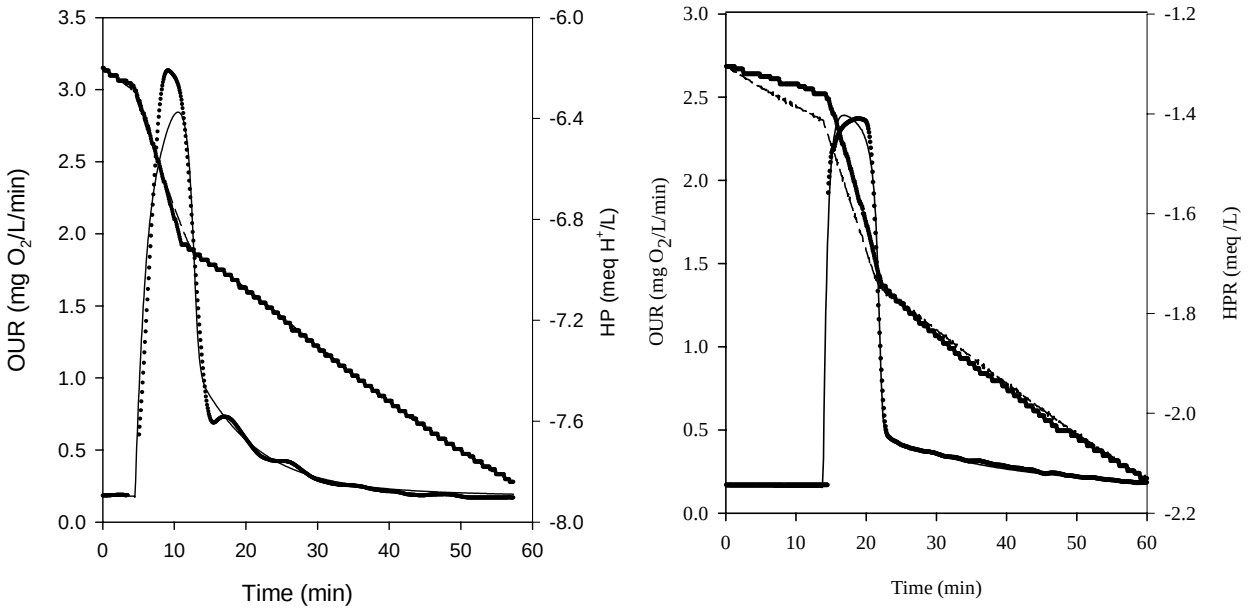

Figure V.D7 Simulateds and experimental profiles for experiment V.D5. Experimental values (dotted), Modelled OUR (solid), modelled HPR (dashed)

As can be observed, the model predicts reasonably well the respirometric and titrimetric profiles, except fort the titrimetric profile of experiment V.D5. The parameter estimation values are shown in Table V.D7.

Table V.D7 Parameter estimation results for experiments V.D4 and V.D5

Parameters	Experiment V.D4	Confidence Interval*	Experiment V.D5	Confidence Interval**
Parameters estimated				
q_{MAX} (1/d)	11.05	0.1%	8.04	0.03%
f_{STO} (g COD_S/g COD_S)	0.43	0.5%	0.43	0.2%
δ (mol/mol)	2.83	0.2%	2.59	0.08%
K_S (mg COD_X/L)	4.1	0.4%	1.55	0.34%
K_1 (g COD/g COD)	0.034	1.03%	0.43	0.5%
K_2 (g^2 COD/g^2 COD)	$2.7 \cdot 10^{-4}$	1.5%	$0.5 \cdot 10^{-4}$	4.8%
τ (min)	2.65	1.14%	0.64	0.17%
pK1	6.04	0.01%	6.09	0.02%
TIC(0) (mmol /L)	2.04	0.03 %	1.13	0.2 %
Parameters assumed				
b_H (1/d)	0.2		0.2	
b_{STO} (1/d)	0.2		0.2	
$X_{STO}(0)$ (g COD_{STO}/L)	1		1	
f_{XI}(g COD/g COD)	0.2		0.2	
Parameters calculated				
$X_H(0)$ (mg COD_X/L)	1600		1400	
$q_{MAX} \cdot X_H(0)$ (mg COD_X/L/d)	8531		5432	
$\mu_{MAX,S}$ (1/d)	8.95		5.49	
k_{STO} (1/d)	8.99		5.66	
$\mu_{MAX,STO}$ (1/d)	8.95		5.49	
Y_{STO} (g COD_{STO}/g COD_{STO})	0.82		0.81	
$Y_{H,S}$ (g COD_X/g COD_S)	0.60		0.58	
$Y_{H,STO}$ (g COD_X/g COD_{STO})	0.71		0.69	

The parameter estimation values obtained are in the expected range of the literature except for the growth rate values which are higher. The value of f_{STO} was casually the same for both experiments. It was a value high enough to describe the storage process, however it was lower than the maximum value of around 0.7 described for WWTP with

high storing capacity biomass. The obtained values of d are in the range of the theoretical values (1-3) as described in Beun *et al.* (2001). As abovementioned, the value of pK1 is lower than 6.36 because of the ionic strength of the medium. This fact is mathematically described in Chapter VI.E when the two-step model is calibrated with respirometric and titrimetric experiments in medium with a known concentration of salts.

The parameter estimation values have been reduced considerably with respect to the experiments in chapter V.C indicating that titrimetric data can be a good tool in view of model calibrating. In any case, the values obtained are too optimistic, probably because of the Q_K estimation as described in the previous section.

V.D.3.3 IMPROVEMENT OF PARAMETER ESTIMATION WITH TITRIMETRIC MEASUREMENTS

In chapter V.C, the model was calibrated using only OUR as measured output with experiment V.C1 (Table V.C3). This experiment showed particularly low storing capacity. Next, the same experiment is calibrated with both respirometric and titrimetric experiments. The graphical results of the calibration are depicted in Figure V.D8 and Table V.D8 compares the parameter estimation results of this experiment with the ones obtained in chapter V.C.

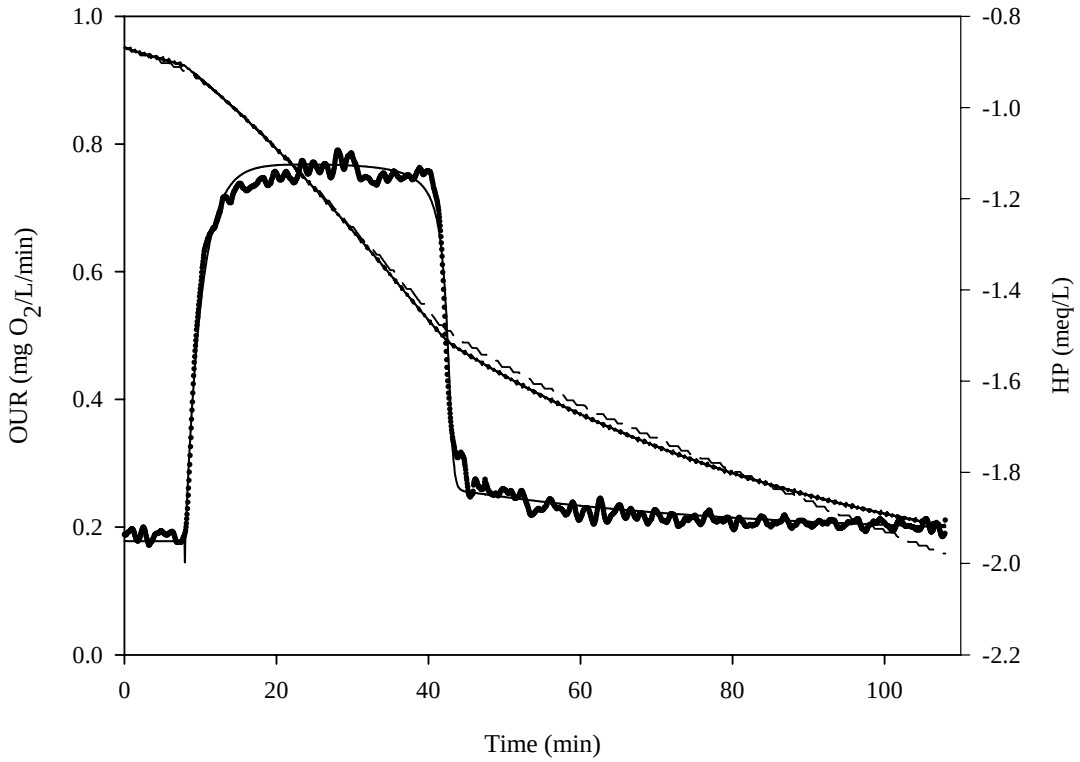

Figure V.D8 Simulateds and experimental profiles for experiment V.C1. Experimental values (dotted), Modelled OUR (solid), modelled HPR (dashed)

Table V.D8 Parameter estimation results for experiment V.C1 with OUR and OUR+HPR

Parameters	OUR	Confidence Interval*	OUR+ HPR	Confidence Interval**
Parameters estimated				
q_{MAX} (1/d)	1.67±0.09	5.4%	1.68±0.02*	0.12%
f_{STO} (g COD_S/g COD_S)	0.29±0.07	24%	0.30±0.03	8.8%
δ (mol/mol)	2.88±0.16	5.6%	2.91±0.05	1.8%
K_S (mg COD_X/L)	0.6±0.4	67%	0.53±0.02	3.5%
K_1 (g COD/g COD)	0.015±0.029	193%	0.02±0.009	49%
K_2 (g^2 COD/g^2 COD)	$1.7\cdot10^{-4}\pm3\cdot10^{-4}$	182%	$1.9\cdot10^{-4}\pm1\cdot10^{-4}$	64%
τ (min)	2.73±0.12	4.4%	2.06±0.05	5.5%
pK1			6.19±0.001	0.01%
TIC (0) (mmol/L)			0.86±0.001	0.17%
Parameters assumed				
b_H (1/d)	0.2		0.2	
b_{STO} (1/d)	0.2		0.2	
$X_{STO}(0)$ (g COD_{STO}/L)	0.99		0.99	
f_{XI}(g COD/g COD)	0.2		0.2	
Parameters calculated				
$X_H(0)$ (mg COD_X/L)	1650		1650	
$q_{MAX}\cdot X_H(0)$ (mg COD_X/L/d)	2755		5144	
$\mu_{MAX,S}$ (1/d)	0.72		1.3	
k_{STO} (1/d)	0.4		3.31	
$\mu_{MAX,STO}$ (1/d)	0.72		1.3	
Y_{STO} (g COD_{STO}/g COD_{STO})	0.83		0.81	
$Y_{H,S}$ (g COD_X/g COD_S)	0.61		0.58	
$Y_{H,STO}$ (g COD_X/g COD_{STO})	0.71		0.68	

As can be observed, the parameter estimation values slightly changed from both calibrations. However, the parameter estimation error was considerably decreased due to the introduction of this new measured variable. Hence, it can be concluded that from a modelling point of view, HP can improve the calibration of the biological COD removal model.

CHAPTER V.D Conclusions

- Titrimetric measurements are a very useful tool for monitoring the biological COD removal process if the effect of the carbon dioxide stripping is taken into account.

- Titrimetric measurements provide valuable information about the substrate depletion point and the process rate complementary to the OUR measurement.

- These techniques are only significant if the substrate is VFA or a dissociated compound. Experiments with ethanol or methanol have demonstrated HP is not influenced by substrate presence.

- Theoretically, titrimetric data could be also used as a tool for quantifying the amount of substrate consumed. The same moles of protons than moles of substrate taken up should be added to system to maintain the pH at a certain setpoint value. However, it has been experimentally observed that the ratio of moles of protons added to moles of substrate taken up is lower than one.

- Finally, these measurements are very useful in view of model calibration since they provide complementary information and reduce the parameter confidence intervals.

CHAPTER VI

BIOLOGICAL NITROGEN OXIDATION

CHAPTER VI.A

Model development for the two-step nitrification process

Part of this chapter is in preparation for submission to Biotechnology and Bioengineering

ABSTRACT

This chapter describes the development of the whole two-step nitrification model involving both ammonia oxidising and nitrite oxidising populations. This description includes the elementary mass and reduction balances to obtain the corresponding stoichiometric coefficients and the deduction of the kinetics of each process. This model is designed to be calibrated using both respirometric and titrimetric data, hence, the prediction of the proton production/consumption is also developed for each of the processes. This chapter also includes a discussion section about the hydraulic modelling, where the assumption of Continuous Stirred Tank Reactor (CSTR) for the components in the gas phase (O_2 and CO_2) is examined. Finally, the phenomenon named as acceleration observed in respirometric batch profiles with ammonia as substrate is described and modelled.

VI.A.1 Introduction to nitrification modelling

The nitrification process was first modelled as a single step system where ammonia was oxidised to nitrate based on the assumption that the limiting step was the first oxidation of ammonia to nitrite. This single step modelling was used in the first attempts to nitrification modelling and, nowadays, ASM models, the reference models in the biological nutrient removal field (Henze et al., 2000) still use this approach. Chandran and Smets (2000) showed that single-step models could not describe respirometric batch experiments when the nitrite oxidation was the limiting step.

Hence, in the last years the single-step simplification has been avoided and, nowadays, two-step nitrification models are the most common in the literature (Gee *et al.*, 1990a; Sheintuch *et al.*, 1995; Picioreanu *et al.*, 1997; Ossenbruggen *et al.*, 1996; Nowak *et al.*, 1995;, Chandran and Smets, 2000; Petersen, 2000; Carrera, 2001; Hao *et al.*, 2001; Gapes *et al.*, 2003 or Pratt et al., 2004 among many others). These models are generally calibrated using respirometric batch tests and some include substrate measurements. The identifiability of the model with OUR as sole measurement for these experiments is an important issue, which was deeply studied in Petersen (2000).

Recently, the utilisation of titrimetric measurements to monitor nitrification has improved the knowledge of the process. Titrimetric measurements provide a lot of information since nitrification is a proton producing process. Hence, with only a pH probe and a pH control loop, the process evolution can be easily monitored. Successful applications of titrimetric techniques for nitrification monitoring are Ramadori *et al.*, 1980; Massone *et al.*, 1995, Gernaey *et al.*, 1998; Gernaey *et al.* 1999; Ficara *et al.*, 2003 and Gapes *et al.*, 2003 among others.

The model presented in this thesis is based on the works abovementioned and arises from a critical revision of them. This critical revision is not described in a separate chapter but it is included through the entire chapter VI. In this chapter, this model is developed, its identifiability is examined and the main stoichiometric and kinetic parameters are either estimated or calculated. During this process, each of the obtained results are discussed and compared with the works abovementioned.

The major improvement of the model presented in this thesis is the integration of the dynamic CO_2 system described in the previous chapter to the nitrification process. Hence, the stripping effect can be in considered in any experiment though the CO_2 stripping rate loses linearity due to the operational conditions.

VI.A.2 Process stoichiometry and kinetics

There are two phylogenetically different groups of bacteria that collectively perform nitrification. Thus, this process can be considered a two-step process. Ammonia oxidising biomass (AOB) performs nitritation (i.e. oxidation of ammonia to nitrite) and nitrite oxidising biomass (NOB) performs nitratation (i.e. oxidation of nitrite to nitrate). The processes involved in the two step nitrification model (related to nitrifying biomass) are:

1. Nitritation
2. Ammonium-Ammonia chemical equilibrium
3. Ammonia stripping
4. Nitratation
5. Nitrous acid – Nitrite chemical equilibrium
6. Endogenous process (for AOB and NOB)
7. Carbonic acid-carbonate chemical equilibriums
8. Carbon dioxide stripping
9. Aeration

Next, the stoichiometric coefficients of each of these processes are deduced through elemental balances and the kinetic expressions of each of them are examined.

VI.A.2.1 NITRITATION

Nitritation is the first step of the nitrification process and describes the biological oxidation of ammonium to nitrite. The biomass in charge of this process (i.e. AOB) prefers the unprotonated ammonia form (NH_3) as substrate since ionised species are not easily transported through the membrane (e.g. Suzuki *et al.*, 1974, Anthonisen *et al.*, 1976; Schlegel and Bowien, 1989 or Gapes *et al.*, 2003). However, from a modelling point of view, some authors still consider the protoned form (NH_4^+) as substrate for practical reasons, i.e. it is more easily measurable and the equilibrium NH_3-NH_4^+ can be considered instantaneous.

Selecting the substrate between ionised and non-ionised forms is not really that important in view of process modelling as long as the existing chemical equilibrium between ammonia and ammonium is taken into account. This equilibrium has proven to be so fast that it can be considered instantaneous. In addition, if pH is controlled at a certain set-point value, the equilibrium can easily be accounted. Almost two moles of protons are experimentally produced per each mol of nitrogen oxidised. One mol is produced from the displacement of the chemical equilibrium when a mol of ammonia disappears and almost a mol is produced in the biological oxidation.
The nitritation process stoichiometry is:

$$aNH_3 + bO_2 + cCO_2 \rightarrow CxHyOzNv + dNO_2^- + eH^+ + fH_20 \qquad \text{(VI.A1)}$$

The mass, charge and degree of reduction balances of the process correspond to the set of equations VI.A2 (a-e):

$$\text{N)}\ a = v + d \qquad \text{(VI.A2a)}$$
$$\text{C)}\ c = x \qquad \text{(VI.A2b)}$$
$$\text{H)}\ 3a = y + e + 2f \qquad \text{(VI.A2c)}$$
$$\text{charge)}\ e - d = 0 \qquad \text{(VI.A2d)}$$
$$\text{degree of reduction)}\ a\cdot(0) + b\cdot(-4) + c\cdot(0) = \gamma_x + d\cdot(-6) + e\cdot(0) + f\cdot(0) \qquad \text{(VI.A2e)}$$

As this expression was developed in C-mol basis, it could be assumed x = 1. The balance of the degree of reduction was developed with NH_3 as N-compound reference (Roels 1983, Heijnen, 1999). Once the biomass composition was known, there were 6 unknown variables (a-f) and only 5 equations, which made the system unsolvable, unless an extra

restriction or equation was obtained. This degree of freedom was the biomass yield (i.e. the moles of carbon biomass formed for each mol of nitrogen consumed). This definition allowed two different interpretations depending whether it was considered the total nitrogen taken up or only the nitrogen oxidised. This choice had a strong effect in the experimental yield assessment from batch respirometric experiments (see section VI.B.2). In this thesis, the yield was defined as the moles of carbon biomass formed per each mol of N-NO_2^- formed (i.e. mol of N-NH_4^+ oxidised).

Hence, d= $1/Y_{A,C}$ where $Y_{A,C}$ (moles C_X/moles N-NO_2^-). Then, solving equations VI.A2, equation VI.A1 became VI.A3:

$$\left(\frac{1}{Y_{A,C}}+v\right)NH_3+\left(\frac{1.5}{Y_{A,C}}-\frac{\gamma_X}{4}\right)O_2+CO_2\longrightarrow CHyOzNv+\left(\frac{1}{Y_{A,C}}\right)NO_2^-+\left(\frac{1}{Y_{A,C}}\right)H^+ +\left(\frac{1}{Y_{A,C}}+\frac{3}{2}v-\frac{y}{2}\right)H_2O \quad \text{(VI.A3)}$$

The stoichiometric coefficients of ammonia, oxygen, biomass and nitrite could be converted to COD and N weight [eq. VI.A4] assuming that:

- the biomass contained γ_X electron moles.
- one mole of electron corresponded to 8g of COD (likewise to an oxygen mol with 32g and 4 electron moles). Hence $8\gamma_X$ corresponded to the grams of biomass (as COD) per mol of carbon biomass.

$$\frac{14}{8\gamma x}\cdot\left(\frac{1}{Y_{A,C}}+v\right)NH_3+\frac{32}{8\gamma x}\cdot\left(\frac{1.5}{Y_{A,C}}-\frac{\gamma x}{4}\right)O_2+\frac{1}{8\gamma x}CO_2\longrightarrow$$
$$CHyOzNv+\frac{14}{8\gamma x}\cdot\left(\frac{1}{Y_{A,C}}\right)NO_2^-+\frac{1}{8\gamma x}\cdot\left(\frac{1}{Y_{A,C}}\right)H^+ +\cdot\frac{1}{8\gamma x}\cdot\left(\frac{1}{Y_{A,C}}+\frac{3v-y}{2}\right)H_2O \quad \text{(VI.A4)}$$

Equation VI.A5 shows the conversion of the biomass yield in molar units ($Y_{A,C}$) to the yield in weight units (Y_A). $Y_{A,C}$ was substituted for Y_A in equation VI.A6.

$$Y_{A,C} = 14\ Y_A / (8\gamma x) \quad \text{where } Y_A \text{ is g } COD_X/g\ N \quad \text{(VI.A5)}$$

$$\left(\frac{1}{Y_A}+\frac{14v}{8\gamma_X}\right)NH_3+\left(\frac{3.43}{Y_A}-1\right)O_2+\frac{1}{8\gamma_X}CO_2\longrightarrow CHyOzNv+\frac{1}{Y_A}NO_2^-+\frac{1}{14\cdot Y_A}H^+ +\left(\frac{1}{14Y_A}+\frac{3v}{16\gamma x}-\frac{y}{16\gamma x}\right)H_2O \quad \text{(VI.A6)}$$

The percentage of nitrogen in biomass in weight basis (i_{NB}) could be calculated as $14v/8\gamma x$ and, then, the final stoichiometry was obtained [eq. VI.A7]:

$$\left(\frac{1}{Y_A}+i_{NB}\right)NH_3+\left(\frac{3.43}{Y_A}-1\right)O_2+\frac{i_{NB}}{14v}CO_2\longrightarrow CHyOzNv+\frac{1}{Y_A}NO_2^-+\frac{1}{14Y_A}H^+ +\left(\frac{1}{14Y_A}+\frac{3i_{NB}}{28}-\frac{y}{16\gamma x}\right)H_2O \quad \text{(VI.A7)}$$

The nitritation process kinetics was defined for a maximum process rate and two substrate limitations [eq VI.A8].

$$\mu_{MAX_A}\cdot\frac{S_{NH4}}{K_{NH,A}+S_{NH4}}\cdot\frac{S_O}{K_{OA}+S_O}\cdot X_A \quad \text{(VI.A8)}$$

where $K_{NH,A}$ = ammonia affinity constant for AOB (mg N-NH_4^+/L)
K_{OA} = oxygen affinity constant of AOB (mg O_2/L)
S_{NH4} = ammonium concentration (mg N-NH_4^+/L)
S_O = oxygen concentration (mg O_2/L)
X_A = AOB biomass
$\mu_{MAX,A}$ = maximum growth rate of AOB (1/d)

VI.A.2.2 NH_4-NH_3 CHEMICAL EQUILIBRIUM

The stoichiometry of this equilibrium is defined for equation VI.A9:

$$NH_4^+ \Leftrightarrow H^+ + NH_3 \qquad \text{(VI.A9)}$$

Table VI.A1 shows that most of the nitrogen is in the ionised form in the optimum range of nitrification (7-8) using the Henderson-Hasselbach equation [eq. V.A10] for these systems (i.e. monoprotic acids).

$$pH = pKa + \log_{10} \frac{[A-]}{[HA]} \qquad \text{(VI.A10)}$$

Table VI.A1 Percentage of N in ionised and non-ionised form as a function of pH (Considering pKa (NH_4^+) = 9.245)

pH	$[NH_4^+]_{EQ}$	$[NH_4OH]_{EQ}$
7	99.43 %	0.56 %
7.5	98.23 %	1.77 %
8	94.62 %	5.38 %

The process kinetics is described in the next set of equations VI.A11 (in molar basis)

$$r_{NH_4^+} = k_{-3} \cdot [NH_3][H^+] - k_3 [NH_4^+] \qquad \text{(VI.A11a)}$$

$$r_{NH_4^+} = \frac{k_3}{K_3} \cdot [NH_3][H^+] - k_3 [NH_4^+] \qquad \text{(VI.A11b)}$$

The kinetic expressions for each compound in molar basis are [eqs VI.A12]:

$$r_{NH_4^+} = k_3 \cdot \left([NH_3] 10^{pK3-pH} - [NH_4^+]\right) \qquad \text{(V1.A12a)}$$

$$r_{NH_3} = -r_{NH_4^+} \qquad \text{(V1.A12b)}$$

$$r_{H^+} = -r_{NH_4^+} \qquad \text{(V1.A12c)}$$

VI.A.2.3 AMMONIA STRIPPING

The systems are generally aerated with conventional air (i.e. without ammonia), so the ammonia stripping should be considered particularly when working at high pH values. For pH values close to neutrality, ammonia stripping should not have any important effect. As in similar cases, the higher resistance to the transfer is considered to be in the liquid side. Hence, the transfer rate is defined by [eq. VI.A13]:

$$r_{NH3} = k_L a_{NH3} \cdot (S_{NH3}^* - S_{NH3}) \qquad \text{(VI.A13)}$$

where $k_L a_{NH3}$ = global NH_3 transfer constant (1/min)
S_{NH3}^* = NH_3 saturation concentration (mg N- NH_3/L)
S_{NH3} = NH_3 concentration (mg N- NH_3/L)

Musvoto *et al.*, (2000a, b) already described the transfer rate independent of the ammonia in the gas phase since the concentration of the ammonia in the gas phase is usually zero and, hence, $S_{NH3}^* = 0$.

VI.A.2.4 NITRATATION

Nitratation is the second step of the nitrification process and describes the biological oxidation of nitrite to nitrate. The biomass in charge of this process is the nitrite oxidising biomass, which is supposed to use the nitrous acid (instead the nitrite anion) likewise in the nitritation process. Two different scenarios appear depending on which N-source is considered: ammonia or nitrous acid. Experimental evidences suggest that the latter can be used as nitrogen source, since some experimental studies are performed with the only addition of nitrite (e.g. Jubany *et al.*, 2004). Moreover, Wallace and Nicholas (1968) affirmed that biomass can incorporate nitrogen in nitrite (or nitrous) form. Nevertheless, it is accepted that the ammonia traces present in the medium are enough for the NOB to grow. In any case, different stoichiometric expressions can be deduced for each scenario:

Ammonia as N-source

If ammonia was considered as the N-source for NOB, the nitratation stoichiometry would be [eq. VI.A14]:

$$aHNO_2 + bO_2 + cCO_2 + dNH_3 \rightarrow CxHyOzNv + eNO_3^- + fH^+ + gH_2O \qquad \text{(VI.A14)}$$

The mass, charge and degree of reduction balances of the process correspond to equations VI.A15 (a-e):

$$N)\ a + d = v + e \qquad \text{(VI.A15a)}$$
$$C)\ c = x \qquad \text{(VI.A15b)}$$
$$H)\ a + 3d = y + f + 2g \qquad \text{(VI.A15c)}$$
$$\text{charge})\ 0 = f - e \qquad \text{(VI.A15d)}$$
$$\text{degree of reduction})\ a\cdot(-6) + b\cdot(-4) + c\cdot(0) + d\cdot(0) = \gamma_x + e\cdot(-8) + f\cdot(0) + g\cdot(0) \qquad \text{(VI.A15e)}$$

As this expression was developed in C-mol basis, it could be assumed x = 1. The balance of the degree of reduction was developed with NH_3 as N-compound reference (Roels 1983, Heijnen, 1999). Once the biomass composition was known, a set of 5 equations with 7 unknown variables was obtained. This system could not be solved since it had two degrees of freedom. The first degree of freedom was the biomass growth yield likewise the nitritation process. Hence, $e = 1/Y_{N,C}$ where $Y_{N,C}$ (moles C_X/moles N-NO_2^-). The other degree of freedom was a system constraint that ammonia was uniquely used as nitrogen source, which was mathematically represented as d = v. The solution of the system was [eq. VI.A16]:

$$\frac{1}{Y_{N,C}}HNO_2 + \left(\frac{0.5}{Y_{N,.C}} - \frac{\gamma_X}{4}\right)O_2 + CO_2 + v\cdot NH_3 \longrightarrow CHyOzNv + \frac{1}{Y_{N,C}}NO_3^- + \frac{1}{Y_{N,C}}H^+ + \frac{3v-y}{2}H_2O \qquad \text{(VI.A16)}$$

The stoichiometric coefficients of the nitrous acid, oxygen, ammonia, biomass and nitrite could be converted to COD and N weight units [eq. VI.A17] as done in equation VI.A4:

$$\frac{14}{8\gamma x\cdot Y_{N,C}}HNO_2 + \frac{32}{8\gamma x}\cdot\left(\frac{0.5}{Y_{N,C}} - \frac{\gamma x}{4}\right)O_2 + \frac{1}{8\gamma_X}CO_2 + \frac{14v}{8\gamma x}\cdot NH_3 \longrightarrow$$
$$CHyOzNv + \frac{14}{8\gamma x\cdot Y_{N,C}}NO_3^- + \frac{1}{8\gamma x}\cdot\left(\frac{1}{Y_{N,C}}\right)H^+ + \frac{1}{8\gamma x}\cdot\left(\frac{3v-y}{2}\right)H_2O \qquad \text{(VI.A17)}$$

Equation VI.A18 shows the conversion of the biomass yield in molar units ($Y_{N,C}$) to the yield in weight units (Y_N) and equation VI.A19 shows the substitution.

$$Y_{N,C} = 14\ Y_N / (8\gamma_X) \text{ where } Y_N \text{ is g } COD_X/gN \qquad \text{(VI.A18)}$$

$$\frac{1}{Y_N}HNO_2 + \left(\frac{1.14}{Y_N} - 1\right)O_2 + \frac{1}{8\gamma x}CO_2 + \frac{14v}{8\gamma x}NH_3 \longrightarrow CHyOzNv + \frac{1}{Y_N}NO_3^- + \left(\frac{1}{14Y_N}\right)H^+ + \frac{1}{8\gamma x}\cdot\left(\frac{3v-y}{2}\right)H_2O \quad \text{(VI.A19)}$$

The percentage of nitrogen in biomass in weight basis (i_{NB}) could be calculated as $14v/8\gamma x$ and, then, the final stoichiometry was obtained [eq. VI.A20]:

$$\frac{1}{Y_N}HNO_2 + \left(\frac{1.14}{Y_N} - 1\right)O_2 + \frac{i_{NB}}{14v}CO_2 + i_{NB}NH_3 \longrightarrow CHyOzNv + \frac{1}{Y_N}NO_3^- + \frac{1}{14Y_N}H^+ + \left(\frac{3i_{NB}}{28} - \frac{y}{16\gamma x}\right)H_2O \quad \text{(VI.A20)}$$

The nitratation kinetics with ammonia as nitrogen source was defined with a maximum process rate and substrate limitations [eq. VI.A21]. The limitations for ammonia are often neglected since it is considered that small traces are enough for NOB biomass to grow. However, if this factor was not considered in view of process simulation, the nitratation would occur in medium without ammonia and, then, ammonia concentration would become negative.

$$\mu_{MAX_N}\cdot\frac{S_{NO2}}{K_{NO}+S_{NO2}}\cdot\frac{S_{NH4}}{K_{NH,N}+S_{NH4}}\frac{S_O}{K_{ON}+S_O}\cdot X_N \quad \text{(VI.A21)}$$

where $K_{NH,N}$ = ammonia affinity constant of NOB (mg N-NH_4^+/L)
K_{NO} = nitrite affinity constant of NOB (mg O_2/L)
K_{ON} = oxygen affinity constant of NOB (mg O_2/L)
S_{NH4} = ammonium concentration (mg N-NH_4^+/L)
S_{NO2} = nitrite concentration (mg N-NO_2^-/L)
S_O = oxygen concentration (mg O_2/L)
X_N = NOB biomass
$\mu_{MAX,N}$ = maximum growth rate of NOB (1/d)

Nitrous acid as N-source

If nitrous acid was considered as the N-source for NOB, the process stoichiometry would be [eq VI.A22]:

$$aHNO_2 + bO_2 + cCO_2 \rightarrow CxHyOzNv + dNO_3^- + eH^+ + fH_20 \quad \text{(VI.A22)}$$

The mass, charge and degree of reduction balances of the process correspond to equations VI.A23 (a-e):

N) $a = v + d$ (VI.A23a)
C) $c = x$ (VI.A23b)
H) $a = y + e + 2f$ (VI.A23c)
charge) $0 = -d + e$ (VI.A23d)
degree of reduction) $a\cdot(-6) + b\cdot(-4) + c\cdot(0) = \gamma_x + d\cdot(-8) + e\cdot(0) + f\cdot(0)$ (VI.A23e)

As this expression was developed in C-mol basis, it could be assumed x = 1. The balance of the degree of reduction was developed with NH_3 as N-compound reference (Roels 1983, Heijnen, 1999). Once the biomass composition was known, a set of 5 equations with 7 unknown variables was obtained. A set of 5 equations with 6 unknown parameters was obtained. The degree of freedom was solved with the biomass yield. Likewise the nitritation process, the biomass yield ($Y_{N,C}$) was defined as the moles of C-biomass formed per mole of nitrogen oxidised (mole of nitrate formed). Hence, $d = 1/Y_{N,C.}$

Expression VI.A24 was obtained solving the balances:

$$\left(\frac{1}{Y_{N,C}}+v\right)HNO_2+\left(0.5\left(\frac{1}{Y_{N,C}}+v\right)-\frac{\gamma x}{4}\right)O_2+CO_2\longrightarrow CHyOzNv+\frac{1}{Y_{N,C}}NO_3^-+\frac{1}{Y_{N,C}}H^++\left(\frac{v-y}{2}\right)H_2O \quad \text{(VI.A24)}$$

The stoichiometric coefficients of the nitrous acid, oxygen, ammonia, biomass and nitrite could be converted to COD and N weight units [eq. VI.A25] as done in equation VI.A4:

$$\frac{14}{8\gamma x}\left(\frac{1}{Y_{N,C}}+v\right)HNO_2+\frac{32}{8\gamma x}\cdot\left(0.5\left(\frac{1}{Y_{N,C}}+v\right)-\frac{\gamma x}{4}\right)O_2+\frac{1}{8\gamma x}CO_2\longrightarrow$$
$$CHyOzNv+\frac{14}{8\gamma x}\cdot\frac{1}{Y_{N,C}}NO_3^-+\frac{1}{8\gamma x}\frac{1}{Y_{N,C}}H^++\frac{1}{8\gamma x}\cdot\left(\frac{v-y}{2}\right)H_2O \quad \text{(VI.A25)}$$

Equation VI.A26 shows the conversion of the biomass yield in molar units ($Y_{N,C}$) to the yield in weight units (Y_N) and equation VI.A27 shows the substitution.

$$Y_{N,C} = 14\ Y_N / (8\gamma x) \quad \text{where } Y_N \text{ is g } COD_X/g\ N \quad \text{(VI.A26)}$$

$$\left(\frac{1}{Y_N}+\frac{14v}{8\gamma_X}\right)HNO_2+\left(\frac{1.14}{Y_N}-1+\frac{2v}{\gamma_X}\right)O_2+\frac{1}{8\gamma_X}CO_2\longrightarrow CHyOzNv+\frac{1}{Y_N}NO_3^-+\frac{1}{14Y_N}H^++\frac{1}{8\gamma_X}\left(\frac{v-y}{2}\right)H_2O \quad \text{(VI.A27)}$$

The percentage of nitrogen in biomass in weight basis (i_{NB}) could be calculated as $14v/8\gamma x$ and, then, the final stoichiometry was obtained [eq. VI.A28]:

$$\left(\frac{1}{Y_N}+i_{NB}\right)\cdot HNO_2+\left(1.14\cdot\left(\frac{1}{Y_N}+i_{NB}\right)-1\right)O_2+\frac{i_{NB}}{14v}CO_2\longrightarrow CHyOzNv+\frac{1}{Y_N}\cdot NO_3^-+\frac{1}{14Y_N}H^++\frac{i_{NB}}{14v}\left(\frac{v-y}{2}\right)H_2O \quad \text{(VI.A28)}$$

The nitratation kinetics with nitrite as nitrogen source is defined with a maximum process rate and substrate limitations [eq. VI.A29].

$$\mu_{MAX_N}\cdot\frac{S_{NO2}}{K_{NO}+S_{NO2}}\cdot\frac{S_O}{K_{ON}+S_O}\cdot X_N \quad \text{(VI.A29)}$$

The first option (ammonia as nitrogen source) was considered in this thesis assuming that traces of ammonia were always present in the medium.

VI.A.2.5 NITROUS ACID CHEMICAL EQUILIBRIUM

The process stoichiometry was defined by equation VI.A30.

$$HNO_2+H_2O\Leftrightarrow H^++NO_2^- \quad \text{(VI.A30)}$$

Most of the nitrogen was present in the ionised form in the pH range where nitrification is optimal (i.e. between 7 and 8) because pKa of nitrous acid is 3.4.The process kinetics in molar basis is described in the next set of equations (VI.A31)

$$r_{HNO_2}=k_{-4}\cdot[NO_2^-][H^+]-k_4[HNO_2] \quad \text{(VI.A31a)}$$

$$r_{HNO_2}=\frac{k_4}{K_4}\cdot[NO_2^-][H^+]-k_4[HNO_2] \quad \text{(VI.A31b)}$$

The kinetic expressions for each compound in molar basis are [eqs VI.A32]:

$$r_{HNO_2} = k_4 \cdot \left(\left[NO_2^- \right] 10^{pK4-pH} - \left[HNO_2 \right] \right) \quad \text{(VI.A32a)}$$

$$r_{NO_2^-} = -r_{HNO_2} \quad \text{(VI.A32b)}$$

$$r_{H^+} = -r_{HNO_2} \quad \text{(VI.A32c)}$$

VI.A.2.6 ENDOGENOUS PROCESS

The endogenous process is a lumped effect of many different processes such as biomass decay, internal polymers degradation, predation or lysis (Keesman *et al.*, 2000; van Loosdrecht and Henze, 1999). The endogenous process stoichiometry is difficult to determine as it depends a lot on the existing population. However, a common assumption is to consider the endogenous process as the biomass decay [eq VI.A33]:

$$CxHyOzNv + aO_2 \rightarrow bCO_2 + cNH_3 + dH_20 \quad \text{(VI.A33)}$$

The system balances are represented in equations VI.A34 a-d

N) v= c (VI.A34a)
C) x = b (VI.A34b)
H) y = 3c + 2d (VI.A34c)
Degree of reduction) $\gamma x + a \cdot (-4) = b \cdot (0) + c \cdot (0) + f \cdot (0)$ (VI.A34d)

As this expression was developed in C-mol basis, it could be assumed x = 1. The balance of the degree of reduction was developed with NH_3 as N-compound reference (Roels 1983, Heijnen, 1999). Once the biomass composition was known, a set of 4 equations with 4 unknown variables is obtained. This system (without degrees of freedom) can be solved with any extra parameter. Hence, equation VI.A35 arises when solving the balances:

$$CHyOzNv + \frac{\gamma_X}{4} O_2 \longrightarrow CO_2 + v \cdot NH_3 + \left(\frac{y - 3v}{2} \right) H_2O \quad \text{(VI.A35)}$$

The stoichiometric coefficients of oxygen, ammonia and biomass could be converted to COD and N weight units [eq. VI.A36] as done in equation VI.A4:

$$CHyOzNv + O_2 \longrightarrow \frac{1}{8\gamma x} CO_2 + \frac{14v}{8\gamma x} NH_3 + \frac{1}{8\gamma x} \cdot \left(\frac{y - 3v}{2} \right) H_2O \quad \text{(VI.A36)}$$

The percentage of nitrogen in biomass in weight basis (i_{NB}) could be calculated as $14v/8\gamma x$ and, then, the final stoichiometry was obtained [eq. VI.A37]:

$$CHyOzNv + O_2 \longrightarrow \frac{i_{NB}}{14v} CO_2 + i_{NB} NH_3 + \left(\frac{y}{16\gamma x} - \frac{3i_{NB}}{28} \right) H_2O \quad \text{(VI.A37)}$$

This process is not totally efficient, since part of the biomass decays in terms of inert fraction. According to the default values of ASM2d (Henze *et al.*, 2000), this fraction is f_{XI} = 0.2. Hence, all the process stoichiometry should by multiplied per: $1\text{-}f_{XI}$ [eq. VI.A38].

$$(1 - f_I) \cdot CHyOzNv + (1 - f_I) \cdot O_2 \longrightarrow \frac{i_{NB}(1 - f_I)}{14v} CO_2 + (1 - f_I) \cdot i_{NB} NH_3 + (1 - f_I) \left(\frac{y}{16\gamma x} - \frac{3i_{NB}}{28} \right) H_2O \quad \text{(VI.A38)}$$

RQ (respiratory quotient) was an interesting parameter to calculate from the process. It represents the molar amount of CO_2 produced per mol of oxygen consumed. According to equation VI.A35, RQ valued $4/\gamma_X$.

As an example, for a default biomass composition ($C_5H_7NO_2$), γx was 4 and, hence, RQ =1. Another commonly used biomass composition is $CH_{1.8}O_{0.5}N_{0.2}$ (Gapes *et al.*, 2003), which had a γx value of 4.2 and, hence, RQ = 0.952.

Analysing the endogenous products, two different effects on pH can be observed. On the one hand, the CO_2 production acidified the medium and, on the other hand the NH_3 release due to the decay and lysis produced the contrary effect. Anyway, the CO_2 production is 5 times higher (1 versus v on VI.A35) in molar basis and the medium basification due to the NH_3 release should not be observed.

The endogenous kinetics is commonly accepted as a decay constant multiplying the biomass [eqs VI.A39a,b].

$$\text{For AOB: } r_{END} = b_A \cdot X_A \text{ and NOB: } r_{END} = b_N \cdot X_N \qquad \text{(VI.A39a,b)}$$

where b_A = decay rate of AOB (1/d)
b_N = decay rate of NOB (1/d)

VI.A.2.7 CARBONIC ACID-CARBONATE EQUILIBRIUM

The carbonic acid-carbonate stoichiometry is depicted in equation VI.A40:

$$CO_2(g) + H_2O \Leftrightarrow H_2CO_3 \Leftrightarrow H^+ + HCO_3^- \Leftrightarrow 2H^+ + CO_3^{2-} \qquad \text{(VI.A40)}$$

Hence, neglecting the second deprotonation of the carbonic acid because the pH working range is 7.5-8.5 and taking into account the reaction between CO_2 and hydroxyl ions, two different equilibriums were considered (Sperándio and Paul, 1997).

$$\begin{aligned} CO_2 + H_2O &\Leftrightarrow H^+ + HCO_3^- \\ CO_2 + OH^- &\Leftrightarrow HCO_3^- \end{aligned} \qquad \text{(VI.A41a,b)}$$

The kinetics of this equilibrium has already been detailed in the biological COD removal chapter (section V.B.2.5) as VI.A42:

$$\frac{dS_{CO2}}{dt} = \left(\frac{k_1}{10^{-pK1}}10^{-pH} + \frac{k_2}{10^{-pK2}}\right)S_{HCO3} - \left(k_1 + k_2 10^{pH-14}\right)S_{CO2} \qquad \text{(VI.A42)}$$

where k_1 = forward reaction rate for the first equilibrium (1/d)
k_2 = forward reaction rate for the second equilibrium (1/d)
pK_1 = acid carbonic first acidity constant
pK_2 = acid carbonic second acidity constant
S_{CO2} = dissolved carbon dioxide concentration (mol CO_2/L)
S_{HCO3} = dissolved bicarbonate concentration (mol HCO_3/L)

VI.A.2.8 CARBON DIOXIDE STRIPPING

This process corresponds to the carbon dioxide transfer from the liquid to the gas phase due to the physical equilibrium between the two phases. The carbon dioxide transfer rate (CTR) is described with equation VI.A43. In the experiments developed in this thesis, the amount of CO_2 present in the liquid (S_{CO2}) was generally higher than the carbon dioxide saturation in the interphase. Hence, CTR was negative and CO_2 was stripped.

$$r_{CTR} = k_L a_{CO2} \cdot (S_{CO2}^* - S_{CO2}) \quad \text{(VI.A43)}$$

where $k_L a_{CO2}$ = global CO_2 transfer coefficient (1/min)
S_{CO2}^* = CO_2 saturation concentration (mol CO_2/L)

VI.A.2.9 AERATION

The aeration process provides the necessary oxygen to the liquid phase. The oxygen transfer rate (OTR) was considered to be limited by the liquid side transfer and it the kinetics of this process was:

$$r_{OTR} = k_L a_{O2} \cdot (S_O^* - S_O) \quad \text{(VI.A44)}$$

where $k_L a_{O2}$ = global O_2 transfer coefficient (1/min)
S_O^* = O_2 saturation concentration (mg O_2/L)

VI.A.2.10 SUMMARY OF THE TWO-STEP NITRIFICATION MODEL

Tables VI.A2 and VI.A3 resume the stoichiometry and the kinetics of the processes described above. Only the compounds in the liquid phase are depicted to simplify the table for the reader.

Table VI.A2 Kinetics of the two-step nitrification model

PROCESS	KINETICS
NITRITATION	$\mu_{MAX_A} \cdot \frac{S_{NH4}}{K_{NH,A} + S_{NH4}} \cdot \frac{S_O}{K_{OA} + S_O} \cdot X_A$
NH_3-NH_4^+ EQUILIBRIUM	$k_3 \cdot \left([NH_3] \cdot 10^{pK3-pH} - [NH_4^+] \right)$
NH_3 STRIPPING	$k_L a_{NH3} \cdot (S_{NH3}^* - S_{NH3})$
NITRATATION(1)	$\mu_{MAX_N} \cdot \frac{S_{NO2}}{K_{NO} + S_{NO2}} \cdot \frac{S_{NH4}}{K_{NH,N} + S_{NH4}} \frac{S_O}{K_{ON} + S_O} \cdot X_N$
NITRATATION(2)	$\mu_{MAX_N} \cdot \frac{S_{NO2}}{K_{NO} + S_{NO2}} \cdot \frac{S_O}{K_{ON} + S_O} \cdot X_N$
HNO_2-NO_2^-EQUILIBRIUM	$k_4 \cdot \left([NO_2^-] \cdot 10^{pK4-pH} - [HNO_2] \right)$
AOB ENDOGENOUS	$b_A \cdot X_A$
NOB ENDOGENOUS	$b_N \cdot X_N$
CO_2 EQUILIBRIUM	$\left(k_1 \cdot 10^{pK_1 - pH} + \frac{k_2}{10^{-pK_2}} \right) \cdot S_{HCO3} - \left(k_1 + k_2 \cdot 10^{pH-14} \right) S_{CO2}$
CO_2 STRIPPING	$k_L a_{CO2} \cdot (S_{CO2}^* - S_{CO2})$
AERATION	$k_L a_{O2} \cdot (S_O^* - S_O)$

(1) ammonia as the nitrogen source
(2) nitrous acid as the nitrogen source

Table VI.A3 Stoichiometry of the two-step nitrification model

PROCESS	S_{CO2}	S_{HCO3}	S_{HNO2}	S_{HP}	S_{NH3}	S_{NH4}	S_{NO2}	S_{NO3}	S_{O2}	X_A	X_N	X_I
	mol/L	mol/L	g N/L	mol/L	g N/L				g O_2/L	g COD/L		
NITRITATION	$-\frac{i_{NB}}{14v}$			$\frac{1}{14Y_A}$	$-\left(\frac{1}{Y_A}+i_{NB}\right)$		$\frac{1}{Y_A}$		$-\left(\frac{3.43}{Y_A}-1\right)$	1		
NH_3-NH_4^+ EQUILIBRIUM				1	14	-14						
NH_3 STRIPPING					1							
NITRATATION(1)	$-\frac{i_{NB}}{14v}$		$-\frac{1}{Y_N}$	$\frac{1}{14\cdot Y_N}$	$-i_{NB}$			$\frac{1}{Y_N}$	$-\left(\frac{1.14}{Y_N}-1\right)$		1	
NITRATATION(2)	$-\frac{i_{NB}}{14v}$		$-\left(\frac{1}{Y_N}+i_{NB}\right)$	$\frac{1}{14Y_N}$				$\frac{1}{Y_N}$	$-\left(1.14\left(\frac{1}{Y_N}+i_{NB}\right)-1\right)$		1	
HNO_2-NO_2^- EQUILIBRIUM			-14	1			14					
AOB ENDOGENOUS	$\frac{i_{NB}}{14v}(1-f_{XI})$				$i_{NB}(1-f_{XI})$				$-(1-f_{XI})$	-1		f_{XI}
NOB ENDOGENOUS	$\frac{i_{NB}}{14v}(1-f_{XI})$				$i_{NB}(1-f_{XI})$				$-(1-f_{XI})$		-1	f_{XI}
CO_2 EQUILIBRIUM	-1	1		1								
CO_2 STRIPPING	-1											
AERATION									1			

(1) ammonia as the nitrogen source
(2) nitrous acid as the nitrogen source

VI.A.3 Hydraulic model

Most of the authors in this field consider both liquid and gas phases as a Continuous Stirred Tank Reactor (CSTR) when modelling an aerated bioreactor. This assumption is generally correct for the liquid phase as long as the reactor is well stirred. On the other hand, the assumption may be also correct for the gas phase only in the case of oxygen since the amount oxygen consumed in the bioreactor is negligible when compared to the oxygen flow. There is practically the same amount of oxygen at the inlet than at the outlet of the reactor and the concentration of oxygen in the gas phase is practically constant. However, when dealing with carbon dioxide the assumption is not that straightforward. If carbon dioxide is included as a variable in the model, the assumption of CSTR should be strongly assessed (Sperándio and Paul, 1997). The amount of CO_2 in the gas inlet is very low (0.036 %) and for high CO_2 production levels and low aeration flows, the CO_2 concentration should not be considered constant in the gas phase as in a CSTR. Hence, the gas phase should be modelled as a Continuous Plug Flow Reactor (CPFR) in view of a correct CO_2 description.

If the gas phase is considered as a CSTR, the value of S^*_{CO2} can be considered constant in time. S^*_{CO2} would correspond to the concentration which is in equilibrium with the value of the CO_2 in the gas phase (C_{CO2}) (i.e. the carbon dioxide concentration in the gas outlet). As most of the research groups in the field of biological nutrient removal modelling do not use carbon dioxide measurements in the gas phase, it is a common assumption that the aeration flow is high enough to maintain the concentration of carbon dioxide in the gas constant and equal to the concentration in the inlet (e.g. Sin *et al.*, 2004). Both assumptions (i.e. Gas phase = CSTR and C_{CO2} inlet = C_{CO2} outlet) should be thoroughly confirmed before being used.

The experiments of this thesis (except for those in the hybrid respirometer), were conduced under particularly low airflow conditions. This was done so that the DO level decreased sharply when a pulse of substrate was added. As described in the equipment section (chapter III.1.1), the OUR value was calculated comparing S_O with S_{OE} (see Figure VI.A1).

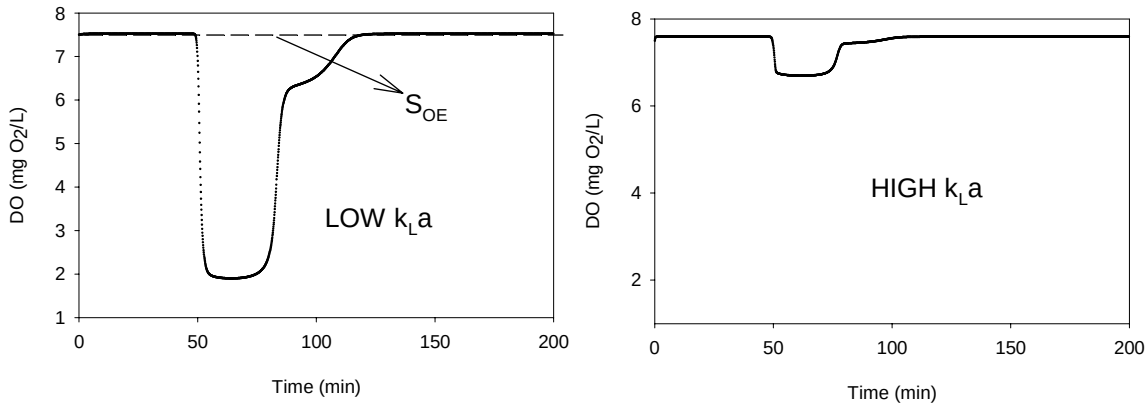

Figure VI.A1 Simulation of a nitrogen pulse (36 mg $N\text{-}NH_4^+$) for high and low k_La values

The lower the k_La was, the lower the oxygen concentration in the reactor for a certain OUR value. Hence, the error in OUR calculation decreased as the differences from S_{OE} and the actual concentration of DO in the reactor increased because the DO measurement error became less important. Under conditions of low k_La (low airflow values), none of the assumptions of gas phase as a CSTR and C_{CO2} inlet = C_{CO2} outlet could be reliably used and, hence, the gas phase in this thesis was considered as a CFPR.

The fact of considering the gas phase as a CFPR caused that the modelling of the system became more complex, since the CO_2 concentration in the gas flow varied along the reactor (in height) and along the time (dynamic process). Thus, solving the two-phase system with one phase working as a CFPR was not a straightforward issue in terms of mathematical modelling (Trambouze *et al.*, 1988; Sperandio and Paul, 1997). Figure VI.A2 shows a schematic picture of the system, where the black colour intensity represents the CO_2 concentration in the gas phase.

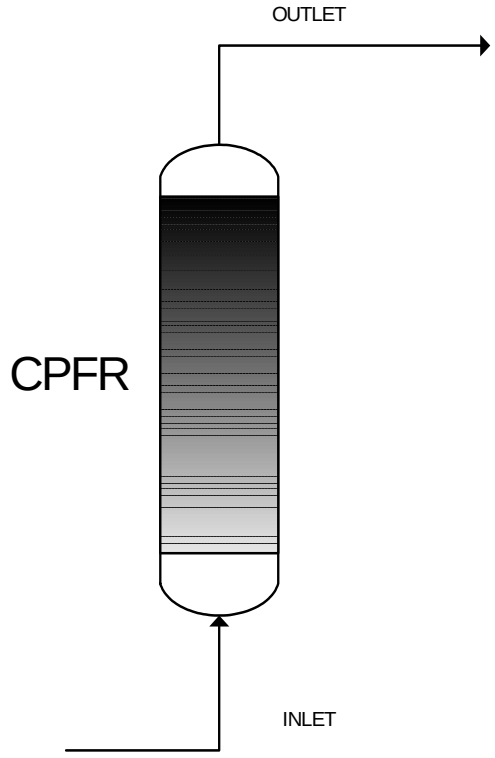

Figure VI.A2 System scheme of the gas phase considered as a CFPR. The colour intensity is proportional to the CO_2 concentration.

Next, the CO_2 balances in both the gas and liquid phases of the reactor are described:

<u>CO_2 balance in the gas phase: CPFR</u>

Equation VI.A45 is the CO_2 balance in the gas phase if it is considered as a CPFR (i.e. in a differential of volume):

$$Q \cdot C_{CO2} + k_L a_{CO2} \cdot (S^*_{CO2} - S_{CO2}) \cdot dV_L = Q \cdot C_{CO2} + \frac{\partial}{\partial z}\left(Q \cdot C_{CO2}\right) dz + \frac{\partial}{\partial t}(C_{CO2} \cdot dV_G) \quad \text{(VI.A45)}$$

where Q= gas flow (L/min)
V_L = Volume of the gas phase (L)
V_G = Volume of the gas phase (L)

Equation VI.A46 derives from substituting $V_L = (1-\varepsilon_G) \cdot V_T$ and $V_G = \varepsilon_G \cdot V_T$ where ε_G stands for the gas hold-up and V_T for the total volume. Moreover S_{CO2}^* is replaced for $C_{CO2} \cdot R \cdot T/H$:

$$k_L a_{CO2} \cdot \left(\frac{C_{CO2}}{H} \cdot R \cdot T - S_{CO2}\right) \cdot (1 - \varepsilon_G) \cdot dV_T = Q \frac{\partial}{\partial z} C_{CO2} \cdot dz + \frac{\partial}{\partial t}(C_{CO2} \cdot \varepsilon_G \cdot V_T) \quad \text{(VI.A46)}$$

where H = Henry's law constant
R = ideal gases constant (0.082 atm·L/mol/K)
T = Temperature (K)

Substituting dV_T for A·dz and Q for A·v

$$k_L a_{CO2} \cdot (\frac{C_{CO2}}{H} \cdot R \cdot T - S_{CO2}) \cdot (1 - \varepsilon_G) \cdot A \cdot dz = A \cdot v \frac{\partial}{\partial z} C_{CO2} \cdot dz + \frac{\partial}{\partial t} (C_{CO2} \cdot \varepsilon_G \cdot A \cdot dz) \qquad \text{(VI.A47)}$$

where A = circulation area (m^2)
v = flow velocity (m/s)

$$k_L a_{CO2} \cdot (\frac{C_{CO2}}{H} \cdot R \cdot T - S_{CO2}) \cdot (1 - \varepsilon_G) = v \frac{\partial}{\partial z} C_{CO2} + \varepsilon_G \cdot \frac{\partial}{\partial t} C_{CO2} \qquad \text{(VI.A48)}$$

Equation VI.A48 describes the variation of carbon dioxide along the time and the reactor height taking into account the stripping from the liquid phase. The value of the carbon dioxide in the liquid phase is very important since it strongly affects the stripping rate value.

A widespread simplification of a CPFR to avoid solving partial derivatives consists of considering the CPFR as the sum of several CSTRs. In this case 10 CSTRs are considered to sum up a whole CPFR as schematised in Figure VI.A3.

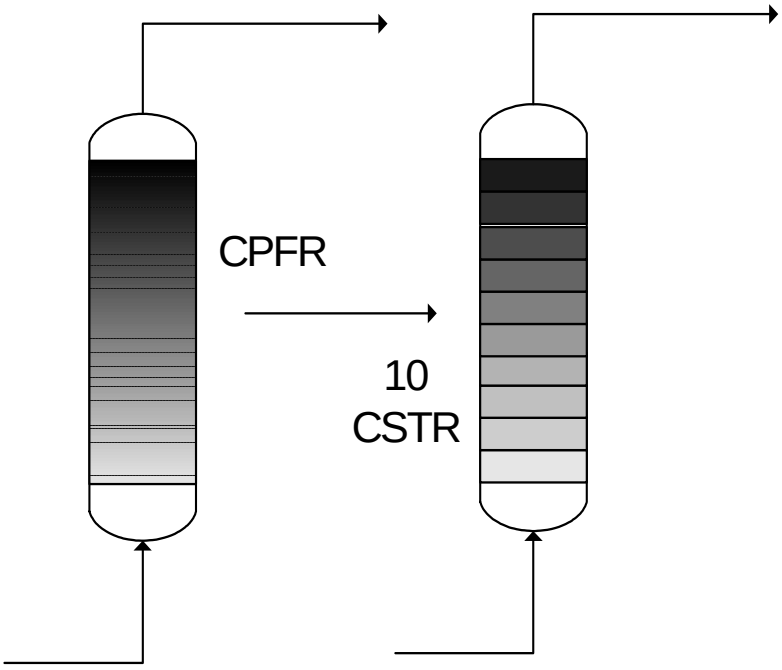

Figure VI.A3 Schematic conversion of one CFPR to 10 CSTR. The colour intensity is proportional to the CO_2 concentration.

Then, the balance in the gas phase is simplified to the next loop of equations:

<u>CO_2 balance in the gas phase : "n" CSTRs</u>

$$Q \cdot C_{CO2}^{i-1} + k_L a_{CO2} \cdot (\frac{C_{CO2}^i}{H} \cdot R \cdot T - S_{CO2}) \cdot V_i \cdot (1 - \varepsilon_G) = Q \cdot C_{CO2}^i + \frac{d}{dt} (C_{CO2}^i \cdot V_i \cdot \varepsilon_G) \qquad \text{(VI.A49)}$$

$$\frac{dC_{CO2}^i}{dt} = \frac{Q \cdot (C_{CO2}^{i-1} - C_{CO2}^i) + k_L a_{CO2} \cdot (\frac{C_{CO2}^i}{H} \cdot R \cdot T - S_{CO2}) \cdot V_i \cdot (1 - \varepsilon_G)}{V_i \cdot \varepsilon_G} \qquad \text{(VI.A50)}$$

CO_2 balance in the liquid phase : CSTR

The CO_2 balance in the liquid phase considers the CO_2 transferred from the gas phase and the biological CO_2 production/consumption (CPR = Carbon Production Rate).

$$\frac{dS_{CO2}}{dt} = -CO_{2\,TRANS} + CPR \qquad \text{(VI.A51)}$$

The CO_2 transferred from the liquid phase to the gas phase considering "n" CSTRs can be calculated according to equation VI.A52:

$$CO2_{TRANS} = \frac{\sum_{i=1}^{n} k_L a_{CO2} \cdot \left(\frac{C^i_{CO2}}{H} \cdot R \cdot T - S_{CO2}\right) \cdot V_i \cdot (1 - \varepsilon_G)}{\sum_{i=1}^{n} V_i \cdot (1 - \varepsilon_G)} \qquad \text{(VI.A52)}$$

VI.A.4 Fast transient initial period: acceleration process

VI.A.4.1 ACCELERATION PROCESS DESCRIPTION

As described in Vanrolleghem *et al.* (2004) important discrepancies appear in short-term batch experiments when comparing the model predictions and the experimental observations, particularly at the start of the experiment (i.e. just after the substrate pulse is added). These discrepancies were explained with the wake-up and the start-up processes.

This situation is also detected for respirometric batch experiments with nitrogen as substrate. Figure VI.A4-left depicts a simulation of the previous two-step model (with default parameter values) without any correction for the initial period. The model predicted a sudden increase to the maximum OUR value once the pulse of ammonia was added. However, figure VI.A4-right depicts an example of an experimental OUR profiles obtained with ammonia as substrate (experiment VI.A1) and shows a clear discrepancy between the experimental and simulated profiles.

Table VI.A4 Experiment VI.A1

EXPERIMENT VI.A1	Comparing simulated and experimental batch OUR profiles
Equipment	BIOSTAT B fermenter (V_0 = 5.5 L)
pH	7.5
Temperature	25 ºC
Acid used	HCl = 0.5 M
Base used	NaOH = 0.25 M
Pulses	200 mg $N\text{-}NH_4^+$ (t = 76 min) -> 36.4 mg $N\text{-}NH_4^+$/L 2g $NaHCO_3$ (t = 0 min)

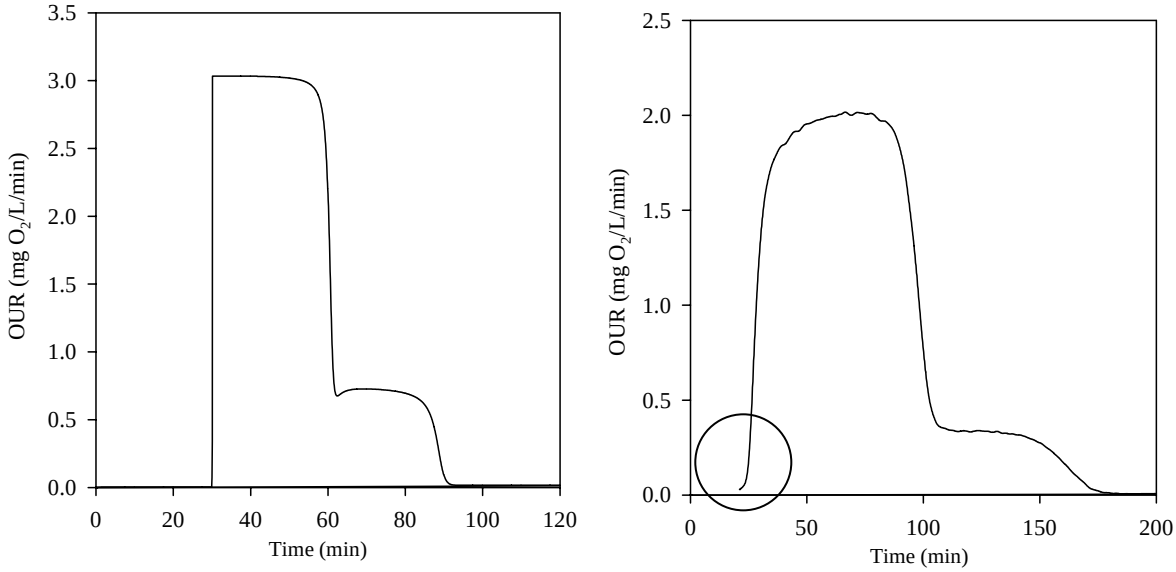

Figures VI.A4 (LEFT) Simulated OUR profile for a 35 mg N-NH_4^+/L pulse and (RIGHT) experimental OUR profile obtained in experiment VI.A1.

However, the case of a nitrogen pulse is different than the case of COD pulse because neither the wake-up nor the start-up could describe correctly the beginning of the OUR profile (indicated with a circle in figures VI.A4 and VI.A5). All respirometric batch tests with ammonia as substrate showed an initial tail which could not be explained with the start-up process. Apparently, the nitritation process was very slow just after the pulse addition and then it speeded up until it reached the maximum rate. This phenomenon has already been described by Smets (personal communication) and they named this phase as acceleration phase. Experiment VI.A2 (Table VI.A5) was conducted to assess whether the acceleration effect was independent of the equipment used. Figure VI.A5 depicts the experimental results for a nitrogen pulse in the LFS respirometer.

Table VI.A5 Experiment VI.A2

EXPERIMENT VI.A2	Acceleration effect on the respirometer
Equipment	LFS respirometer (V_0 = 1 L)
pH	7.5
Temperature	25 ºC
Pulses	30 mg N-NH_4^+ (t = 30 min) -> 30 mg N-NH_4^+/L

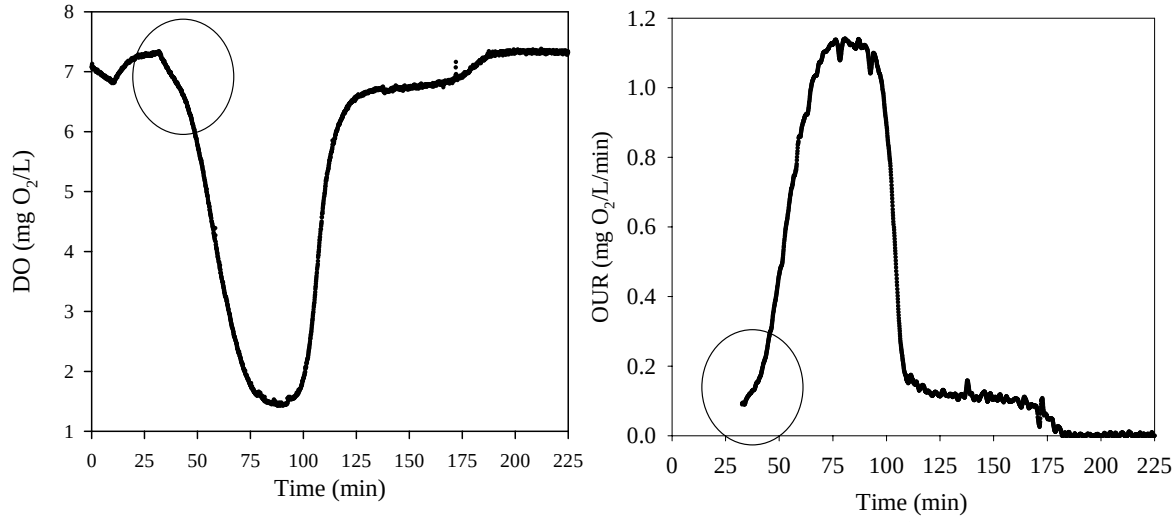

Figures VI.A5 a) respirogram and b) OUR profile for a 30 mg N-NH_4^+/L pulse at the LFS respirometer.

The acceleration phase was observed in all the ammonia batch tests performed in both the respirometer and BIOSTAT equipments. The figure on the left shows the effect observed in a LFS respirogram and the figure in the right indicates how important it becomes when calculating the OUR profile.

Experiment VI.A3 (Table VI.A10) shows that this phenomenon was not only observed in the OUR profile, but also in the ammonium measurements performed.

Table VI.A10 Experiment VI.A3

EXPERIMENT VI.A3	Analysis of acceleration effect on ammonium measurements
Equipment	BIOSTAT B fermenter (V_0 = 5.6 L)
pH	7.5
Temperature	25 ºC
Acid used	HCl = 0.5 M
Base used	NaOH = 0.25 M
Pulses	200 mg N-NH_4^+(t = 76 min) → 35.7 mg N-NH_4^+/L 2g $NaHCO_3$ (t = 0 min)

The experimental results are depicted on Figure VI.A6, which shows how ammonium was first consumed at a very low rate and then it speeded up likewise the OUR. The nitrite profile also indicated this change in the process rate.

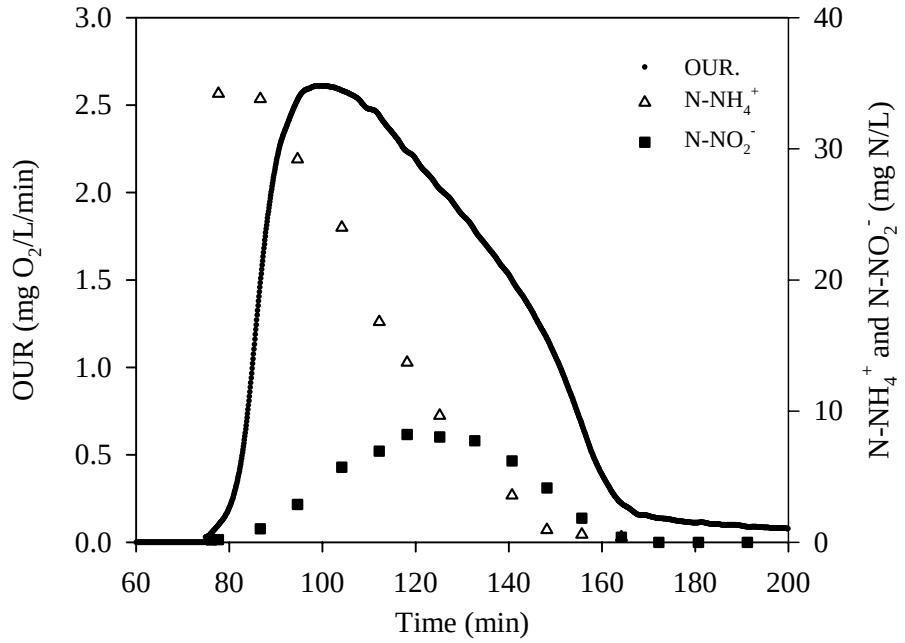

Figure VI.A6 Experimental OUR, ammonium and nitrite profiles showing the accelaration effect.

This initial tail could not be described with a first order delay (start-up), since the start-up process describes convex shapes, whereas in the experimental OUR profiles the curvature changed from concave to convex as can be observed in Figure VI.A7, where the experimental OUR profile shown on Figure VI.A4-right is zoomed. The OUR seemed to grow exponentially in this short initial concave period.

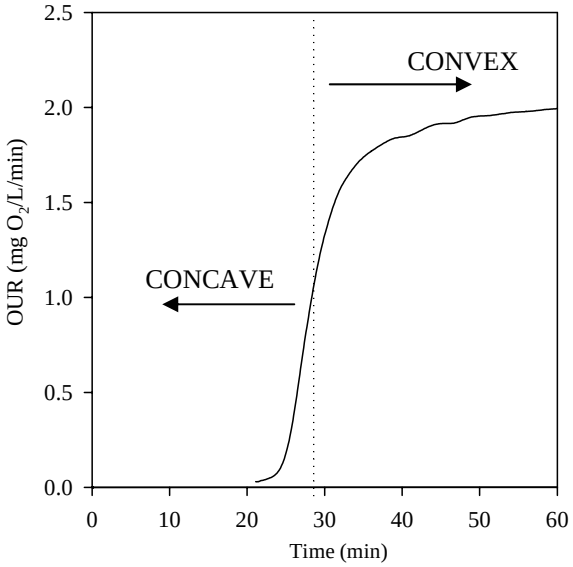

Figure VI.A7 Zoomed acceleration phase of experiment VI.A1.

VI.A.4.2 METABOLIC BASIS FOR THE ACCELERATION PROCESS

Smets (personal communication) held that this acceleration phase is due to the lack of reducing equivalents at the start of the pulse. To understand this assumption, a deeper insight to the nitritation process is required since the elementary biological reactions of nitritation and nitratation showed previously are simplifications of the true catabolic processes. The metabolic processes of nitritation are a common knowledge in the literature: for example: Schlegel and Bowien, (1989) for *Nitrosomonas,* Hagopian and Riley (1998), Poughon *et al.*, (2001) or Arp *et al.*, (2002).

Figure VI.A8 shows a schematic representation of the metabolic processes involved in the nitritation case. The first step in nitritation is the reduction of ammonia to hydroxylamine (NH_2OH) [eq. VI.A53].The enzyme in charge of this process is *ammonia monooxygenase* (AMO). Hydroxilamine is later oxidized to nitrite by *hydroxylamine oxidoreductase* (HAO) [eq. VI.A54].

$$NH_3 + 2H^+ + 2e^- + O_2 \xrightarrow{AMO} NH_2OH + H_2O \qquad \text{(VI.A53)}$$

$$NH_2OH + H_2O \xrightarrow{HAO} NO_2^- + 4e^- + 4H^+ \qquad \text{(VI.A54)}$$

Hence, hydroxylamine could be used directly as a substrate if it wasn't toxic even at very low concentrations (Bock *et al.*, 1991; Frijlink *et al.*, 1992; Hagopian and Riley, 1998). Oxygen is only required in the first step, whereas the second step is a simple four-electron oxidation that uses oxygen derived from water dissociation. As can be observed, the first step requires reducing equivalents which are regenerated in excess in the second step. If the reducing equivalents were limiting, this limitation would disappear once the process started and some hydroxylamine was oxidised. According to this, the nitritation process acts as an autocatalytic reaction, speeding up as electrons are produced in the second nitritation step.

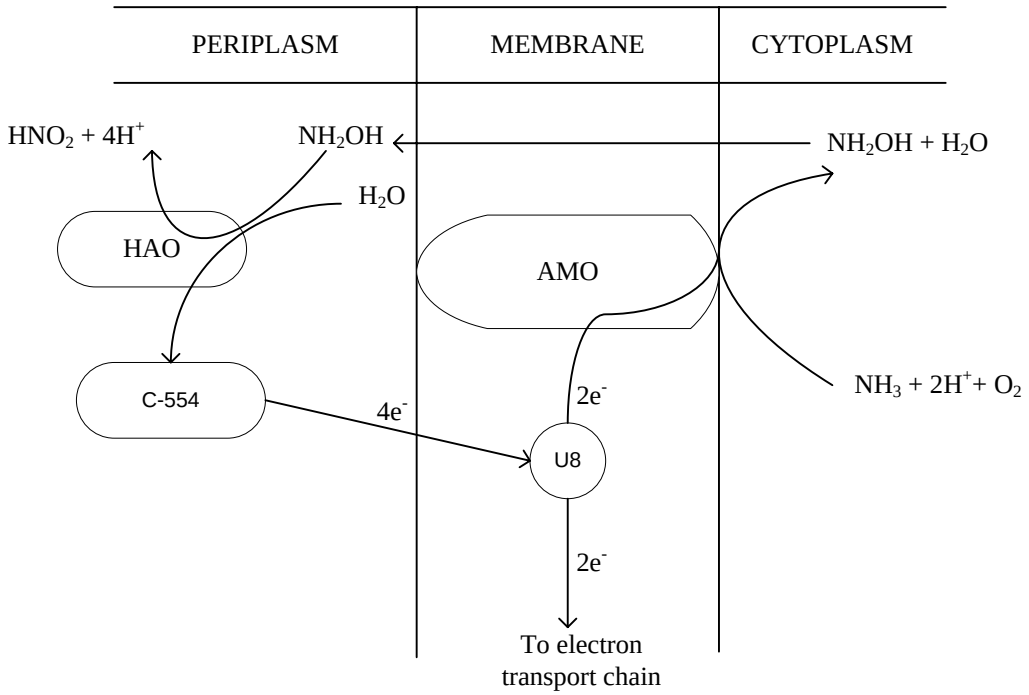

Figure VI.A8 Schematic metabolic representation of the nitritation step (adapted from Schlegel and Bowien, 1989) .C-554 – Cytocrom 554 and U8 – Ubiquinone 8.

Another possibility could be that the AMO enzyme was an allosteric enzyme. Allosteric enzymes often display sigmoidal plots of the reaction velocity versus substrate concentration, rather than the hyperbolic plots predicted by the Michaelis-Menten equation (analogous to Monod equation but for enzymes). In allosteric enzymes, the binding of substrate to one active site can affect the properties of other active sites in the same enzyme molecule. A possible outcome of this interaction between subunits is that the binding of substrate becomes cooperative; that is, the binding of substrate to one active site of the enzyme facilitates substrate binding to the other active sites.

If AMO was allosteric, such cooperation would result in a sigmoidal plot of process rate versus ammonia (i.e. acceleration effect). In addition, the activity of an allosteric enzyme may be altered by regulatory molecules that are reversibly bound to specific sites other than the catalytic sites. The catalytic properties of allosteric enzymes can thus be adjusted to meet the immediate needs of a cell. For this reason, allosteric enzymes are key regulators of metabolic pathways in the cell (AMO regulates the ammonia oxidation pathway).

Deciding which of these two explanations (or others possible) for the acceleration phase was the correct one was beyond the scope of this thesis. However, for "scientific curiosity", a simple experiment was conducted to detect if there was acceleration with nitrite as substrate (experiment VI.A4 - Table VI.A11). According to the lack of reducing power theory, acceleration should not be observed in this case.

Table VI.A11 Experiment VI.A4

EXPERIMENT VI.A4	Acceleration phase with nitrite pulse
Equipment	LFS respirometer (V_0 = 0.8 L)
pH	7.5
Temperature	25 ºC
Acid used	HCl = 0.5 M
Pulses	30 mg $N\text{-}NO_2^-$ (t = 8 min) -> 37.5 mg $N\text{-}NO_2^-/L$

Figure VI.A9 shows that a pulse of nitrite was added and the acceleration effect was not observed. Moreover, this experiment discarded that the experimentally observed acceleration effect was due to any operational cause such as low stirring (i.e. bad homogenization).

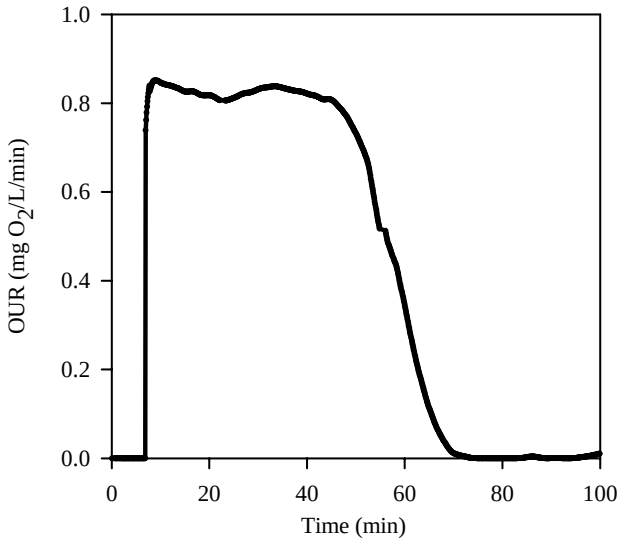

Figure VI.A9 Experimental OUR profile obtained for experiment VI.A4.

VI.A.4.2 ACCELERATION PHASE MODELLING

Experiment VI.A5 (Table VI.A12) was used to assess the effect of neglecting this acceleration phase for modelling purposes and figure VI.A10 shows the experimental results.

Table VI.A12 Experiment VI.A5

EXPERIMENT VI.A5	Acceleration phase quantification
Equipment	LFS respirometer (V_0 = 0.8 L)
pH	7.5
Temperature	25 ºC
Acid used	HCl = 0.25 M
Base used	NaOH = 0.25 M
Pulses	15 mg N-NH_4^+ (t = 50 min) -> 18.75 mg N-NH_4^+/L
	15 mg N-NO_2^- (t= 130 min) -> 18.75 mg N-NO_2^+/L
	0.6 g $NaHCO_3$ (t = 0 min)

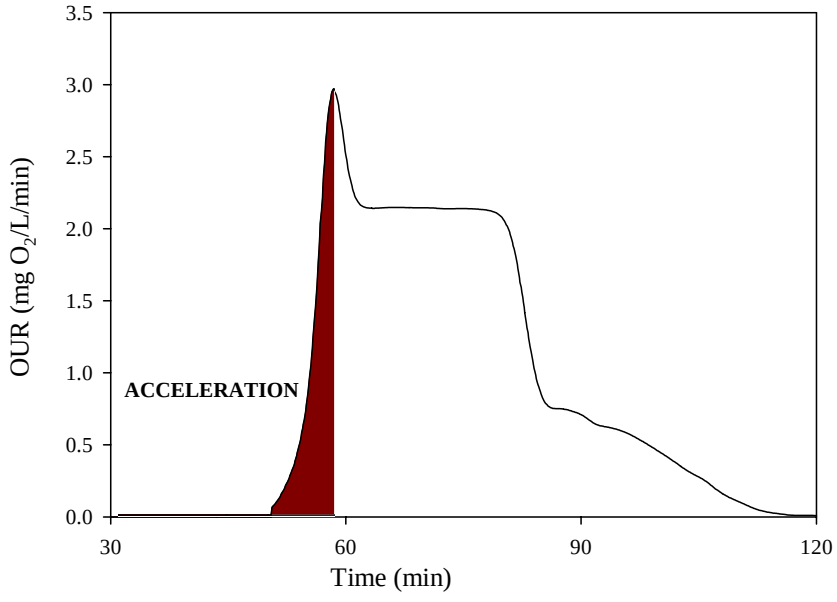

Figure VI.A10 OUR profile obtained for experiment VI.A5 and acceleration phase (filled area).

Figure VI.A10 shows that ignoring the acceleration phase would imply introducing a huge error in parameter estimation using this respirometric experiment. As detailed in the introduction, the area under the OUR profile is proportional to the total oxygen consumption due to the pulse, which is linked to the amount of substrate added by means of the biomass yield. The area filled in Figure VI.A10 corresponds to a 12 % of the total area. Hence, if one thought that the acceleration phase was an experimental error, and deliberately omitted it, the calculated yield value using this pulse would we overestimated since less oxygen consumption would be considered.

On the other hand, some authors use yields which have been previously estimated (or assumed form the literature). Thus, the total oxygen consumption could be exactly calculated supposing the amount of initial substrate added is always known. Figure VI.A11 illustrates the importance of the acceleration and start-up processes in view of modelling. This figure compares the experimental OUR (experiment VI.A5) with a simulation of the two pulses without any consideration to the acceleration or start-up processes. As the k_La was very low, the simulated sharp-peak on the OUR would be exaggerated if the biomass started consuming at its maximum value.

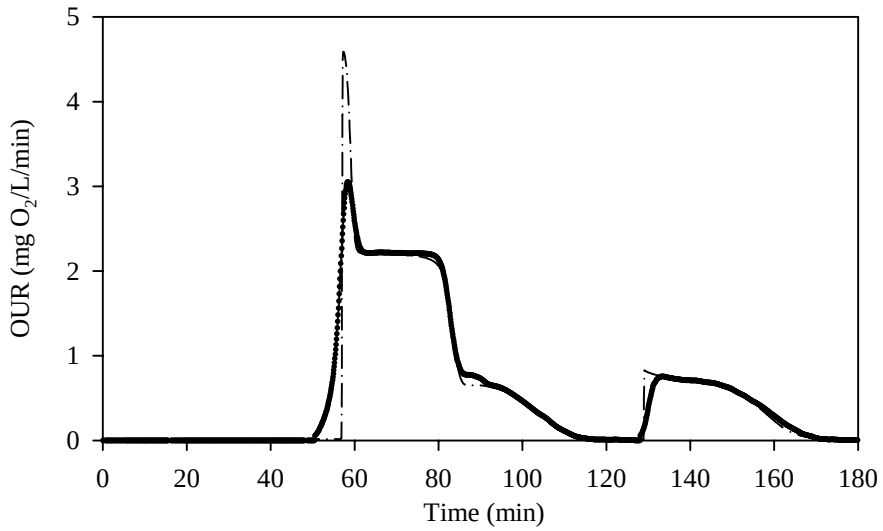

Figure VI.A11 Experimental OUR profiles of VI.A5 (solid) and simulation (dash-dotted) ignoring both the acceleration and the start-up phases.

The purpose of this thesis was to systematically and correctly estimate the nitrification model parameters using short-term experiments. It has been shown that the acceleration phase must be described. However, for this aim, the internal metabolic causes and basis of the acceleration phase and a detailed metabolic description may not be necessary. For a thorough description of the process, new reactions which involve new compounds (i.e. reaction intermediates such as hydroxylamine) would be required. The more processes included, the more parameters to estimate and, with only OUR and HPR as output measurement, these parameters probably could not be identified.

The observed acceleration process should be described with a mathematical simple equation likewise the modelling of the start-up (Vanrolleghem *et al.*, 2004). Due to the change in the curvature, two parameters were required. The first guess was an overdamped second-order system (which may be the next logical step to the first order time delay of the start-up). The response of these systems in front a step input change is a slow initial change and then they pick up speed. It is an S-shape response which may fit the acceleration process. An example of these systems would be two non-interacting material capacities (i.e. two first-order time delays) in series with different time constants (Stephanopoulos, 1990).

The transfer functions for the two delays are:

$$G_1(s) = \frac{K_1}{\tau_1 \cdot s + 1} \qquad G_2(s) = \frac{K_2}{\tau_2 \cdot s + 1} \tag{VI.A55a,b}$$

The overall transfer function is:

$$G_o(s) = \frac{K_o}{(\tau_1 \cdot s + 1)(\tau_2 \cdot s + 1)} \tag{VI.A56}$$

When transformed in time basis the result is:

$$y(t) = K_o \cdot \left[1 + \frac{1}{\tau_2 - \tau_1} \cdot (\tau_1 \cdot e^{-t/\tau_1} - \tau_2 \cdot e^{-t/\tau_2}) \right] \tag{VI.A57}$$

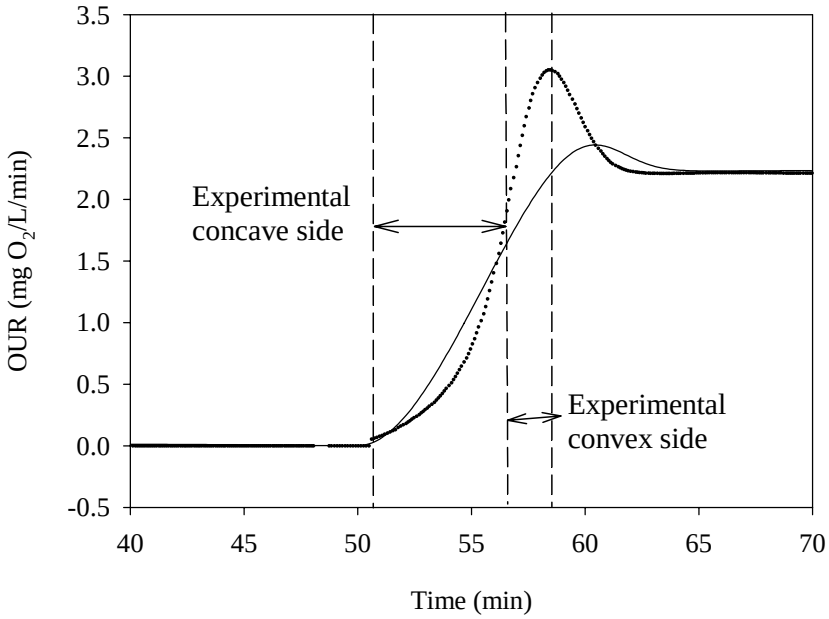

Figure VI.A12 Experimental OUR (dotted) versus modelled OUR (line) profiles. The OUR model is an overdamped second order system.

However, this equation could not be fitted to the observed acceleration process because the second order system is by definition symmetric and the concave part in the acceleration phase was much longer than the convex one. An example of fitting using this second order system is plotted in Figure VI.A12. Then, a new expression for a proper fitting was searched. After some failed attempts (results not shown) an expression based on the Gaussian-like curve was found to be successful (VI.A56)

$$e^{\frac{-(t-\beta)^2}{\psi}} \tag{VI.A58}$$

where β represents the point at the maximum and ψ defines the length of the acceleration phase. By definition, this expression describes a symmetric profile, which slows down after the value of β.

An example of this Gaussian expression for β = 50 and ψ = 10 is depicted in Figure VI.A13.

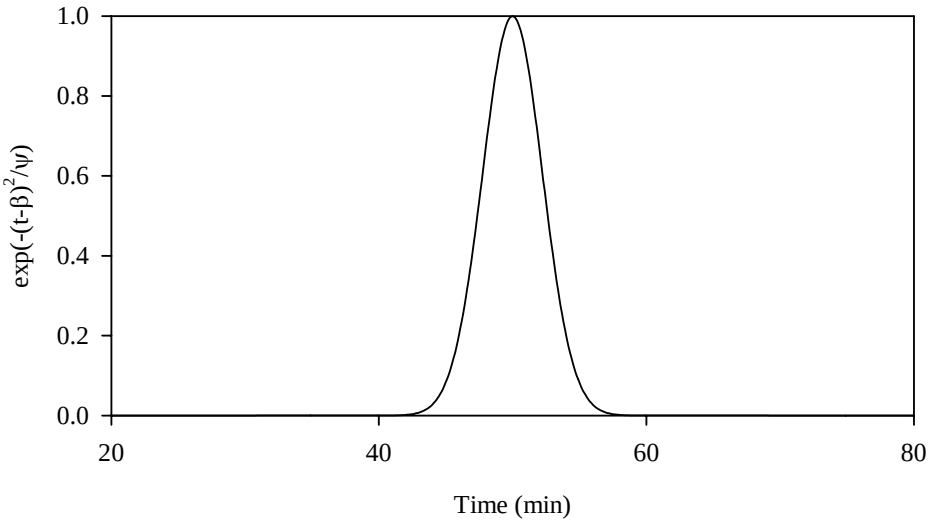

Figure VI.A13 Gaussian-like expression for β = 50 and ψ = 10

However, this expression was not perfect yet since slow substrate consumption was only needed at the start of the pulse. If the whole expression was used, the consumption rate would be slow at the start and also after pulse (because the Gaussian curves are by definition symmetric). This problem was overcome by modelling only half of the Gaussian profile (until the value of β).

Figures VI.A14 and VI.A15 depict the influence of the two parameters of the expression β and ψ on a simulated OUR profile (with default parameters). As can be observed, the value of β indicates the time instant of the end of the acceleration phase and the ψ value describes the curvature of the acceleration process. Nevertheless, this modelling short way will be further discussed in chapter VI.D in the calibration and validation part.

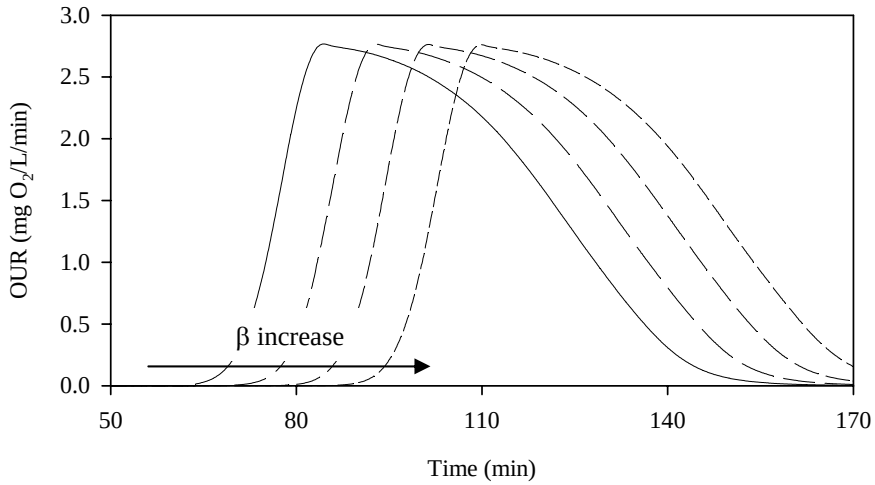

Figure VI.A14 Influence of the β parameter on the simulated OUR profile.

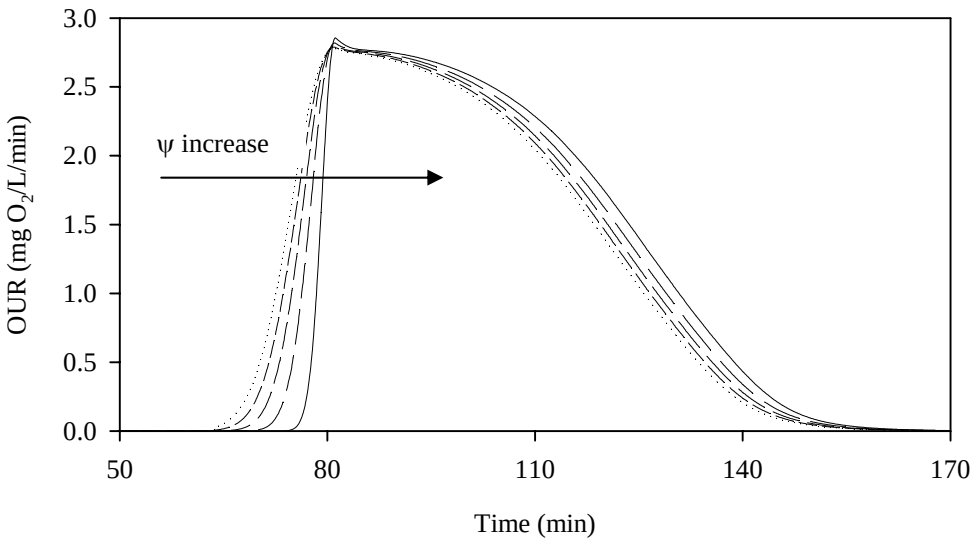

Figure VI.A15 Influence of the ψ parameter on the simulated OUR profile.

Chapter VI.A Conclusions

- A model to describe the main processes involved in the biological nitrogen removal processes has been developed. The stoichiometry of each process has been assessed with mass, charge and degree of reduction balances.

- Two different stoichiometries are required depending whether the N-source for NOB biomass is ammonia or nitrous acid.

- The carbon dioxide equilibrium and stripping processes are necessary to accurately describe the acid/base addition to the system.

- The gas phase was considered as a CPFR to describe the evolution of C_{CO2} along the time and the reactor height since the system worked under low k_La_{CO2} conditions and the hypothesis of CSTR could not be reliably used.

- The phenomenon known as acceleration (i.e. the nitritation process is very slow after the pulse addition and then it speeds up until it reaches the maximum rate) could not be described with an overdamped second order system.

- An expression based on the Gaussian-like curve was found to be successful to describe the acceleration phase.